

FULL WAVEFORM INVERSION FOR COMPLEX NEAR-SURFACE

IMAGING USING SEG SEAM II SYNTHETIC MODEL

BY

Ali Ahmed Hussein Mohamed

A Thesis Presented to the
DEANSHIP OF GRADUATE STUDIES

KING FAHD UNIVERSITY OF PETROLEUM & MINERALS

DHAHRAN, SAUDI ARABIA

In Partial Fulfillment of the
Requirements for the Degree of

MASTER OF SCIENCE

In

GEOPHYSICS

February 2018

KING FAHD UNIVERSITY OF PETROLEUM & MINERALS

DHAHRAN- 31261, SAUDI ARABIA

DEANSHIP OF GRADUATE STUDIES

This thesis, written by **Ali Ahmed Hussein Mohamed** under the direction of his thesis advisor and approved by his thesis committee, has been presented and accepted by the Dean of Graduate Studies, in partial fulfillment of the requirements for the degree of **MASTER OF SCIENCE IN GEOPHYSICS**.



Dr. Abdullatif Al-Shuhail

(Advisor)



Dr. Abdulaziz M. Al-Shaibani

Department Chairman



Dr. Stewart Greenhalgh

(Member)



Dr. Salam A. Zummo

Dean of Graduate Studies



Dr. Sherif Hanafy

(Member)

27/3/18

Date

© Ali Ahmed Mohamed

2018

[To my family

and for the memory of my father]

ACKNOWLEDGMENTS

First and foremost, I would like to thank Allah, whose many blessing has made me who I am today. The following document summarizes years' worth of effort, frustration and achievement. However, there are several peoples who I am indebted for their contributions in this research, study and dissertation of this thesis. I am forever grateful to Dr. Abdullatif Al-Shuhail for having accepted to be my thesis advisor and for his generous support, encouragement and educative discussions. I also express my warmest gratitude to my other supervisors Prof. Stewart Greenhalgh and Dr. Sherif Hanafy who suggested to examine acoustic FWI on viscoelastic data which helps to strengthen the work of this project. I would like to show my greatest appreciation to all KFUPM staff, faculty, my colleagues and friends for their help throughout this journey. Special thanks go to Dr. Abdulaziz M. Al-Shaibani, chairman of Geoscience department for his approval to join this master program and carry out this project using the department facilities. Finally, many thanks to my family for their endless support and encouragement throughout this journey.

TABLE OF CONTENTS

ACKNOWLEDGMENTS	V
TABLE OF CONTENTS	VI
LIST OF TABLES.....	IX
LIST OF FIGURES.....	X
LIST OF ABBREVIATIONS.....	XIII
ABSTRACT	XIV
ملخص الرسالة	XVI
CHAPTER 1: INTRODUCTION	1
1.1 Introduction.....	1
1.2 Hydrocarbon exploration in complex land environments	2
1.3 SEAM Program	4
1.4 Reflection seismology	6
1.5 Thesis Objectives	7
1.6 Thesis overview and contributions.....	8
CHAPTER 2: FWI: THEORY, METHODOLOGY AND TECHNICAL DESCRIPTION....	9
2.1 Numerical modeling.....	9
2.2 Finite difference forward modeling.....	10
2.3 FWI theory	13
2.4 FWI flowchart and methodology.....	14
2.5 FWI technical description.....	16
2.5.1 Forward modeling of the data.....	16

2.5.2	Residual using least square objective function	17
2.5.3	Travel time errors using travel time objective function	17
2.5.4	Cycle skipping and local minimum trapping.....	18
2.5.5	Velocity gradient and model update.....	18
 CHAPTER 3: SEISMIC WAVE PROPAGATION IN THE COMPLEX NEAR SURFACE ...		
.....		20
3.1	Near-surface geology of Arabian Peninsula.....	20
3.2	SEG SEAM Phase II Arid synthetic model.....	22
3.3	Finite difference modeling using FDelmodc software.....	24
3.4	Source wavelet generation	24
3.5	2D line extraction and expansion from SEAM model's parameters	26
3.6	Ways of addressing complex near-surface geology through ray tracing and finite difference modeling.....	28
3.6.1	Ray tracing method	29
3.6.2	Finite difference method.....	34
3.7	Discussion and conclusions	38
 CHAPTER 4: ACOUSTIC FWI ON ACOUSTIC AND VISCOELASTIC SYNTHETIC DATA.....		40
4.1	Requirements for FWI success	40
4.2	FWI workflow	41
4.2.1	Input data preparation	41
4.2.2	Source wavelet.....	42
4.2.3	Starting Model.....	43
4.2.4	Which data to include?	47
4.2.5	Objective function	48
4.2.6	Frequency bands	49
4.2.7	Gradient smoothing	49
4.2.8	Line search.....	50
4.3	Case study-1: Acoustic FWI on acoustic synthetic data.....	52
4.4	Case study-2: Acoustic FWI on viscoelastic synthetic data	55
4.5	Discussion and conclusion.....	60

CHAPTER 5: DISCUSSION AND CONCLUSIONS	61
REFERENCES.....	64
VITAE.....	67

LIST OF TABLES

Table 1: FWI over four frequency bands using refraction or refraction & reflection events with different objective function methods.	49
Table 2: Two synthetic dataset generated with different parameters and attributes, acoustic synthetic data in case-1 and viscoelastic with noise and multiple in case-2.....	52
Table 3: Acoustic FWI was performed over five frequency bands using refraction or refraction & reflection events with different number of iterations.	53

LIST OF FIGURES

Figure 1-1: Map of world oil reserves in land, 2013. Darkness of the blue color indicates the amount of oil reserves.....	3
Figure 1-2: Middle East and North Africa map with Karst regions (shown in magenta) where there are numerous oil exploration activities on land	4
Figure 1-3: Past, present and future SEAM models, presented at SEG October 2014, Phase I represents challenges of sub-salt imaging, Phase II shows land seismic challenges, the objective of Phase III is to advance current methodologies of predrilling pressure and hazards predictions and Phase IV is used to improve the workflows in managing the life of the field.	5
Figure 2-1: A schematic chart shows the relation between forward, inverse and appraisal problems....	10
Figure 2-2: Multi-scale time domain acoustic FWI flowchart. This flow updates the primary velocity by minimizing the difference between predicted and observed data through an iterative process which starts from low frequency and progressively increases the bandwidth of the data.	14
Figure 3-1: Regional geological cross section from west to east of Saudi Arabia (Courtesy of USGS), shows the thickness of the sedimentary rock increases from west to east of Saudi Arabia.....	20
Figure 3-2: Geological stratigraphic column of the Tertiary rocks at eastern of Saudi Arabia (Courtesy of LUKSAR), Tertiary system consist of six main formation which introduces strong velocity contrast due to the intercalation between low velocity (sand and shale) layers and fast velocity (anhydrite, dolomite and limestone) layers.....	21
Figure 3-3: Near-surface of arid model with shallow and deep Karst fields (SEG.org) shows complex velocity variation due to the presence of low velocity karst geobodies and unconsolidated sediment within the bed rock.	22
Figure 3-4: Geological features at top of Arid (a) 3D structural modeling of shallow Karst fill with very slow materials (b) Wadis and buried rivers bed (c) Depth slice of top of the velocity model shows strong velocity heterogeneities (Displays courtesy of Schlumberger WesternGeco. Source is SEG.org)	23
Figure 3-5: Geological features at 200m of Arid model (a) depth slice at 200m through 3D real seismic (b) 3D structural modeling of deeper Karst (c) Depth slice at 200m in the velocity model (Displays courtesy of Schlumberger WesternGeco. Source is SEG.org).	23
Figure 3-6: Klauder wavelet with zero phase spectrum generated (a) Makewave command in su and wavelet attributes (b) the wavelet in time domain (c) amplitude spectrum shows flat spectrum from 3-20Hz.	25
Figure 3-7: 2D line is shown as white solid line over Vp Arid model (a) depth slice at top of the model (b) depth slice at 200m in the model.	26
Figure 3-8: 2D Vp model (a) Original Vp with 10km length (b) Extended Vp with 20km length.	27
Figure 3-9: Arid SEAM model properties, (a) Vp, (b) Vs, (c) rock density and (d) Qp=Qs.	27
Figure 3-10: Four velocity models represent different levels of near-surface complex geology (a) smooth velocity variation (b) strong vertical velocity variation (c) strong spatial and vertical velocity variation (d) Arid SEAM model that has a complex velocity variation including Karst with slow velocity.	28
Figure 3-11: Interface based Arid SEAM model overlaid with raypaths (a) gridded model (b) interface based model overlaid with reflected P-wave rays (c) interface based model overlaid with reflected P-wave rays and 1 st & 2 nd order of multiples (d) interface based model overlaid with reflected P-wave rays and 1 st to 3 rd order of multiples	30

Figure 3-12: 2D view of ray paths colored with offset overlaid over velocity model shows the rays are trapped within low velocity layers (a) smoothed 1D model (b) complex 1D model (c) complex 3D model (d) complex 3D model with Karst.	31
Figure 3-13: Base carbonate horizon shifted down by 200m (a) horizon overlaid with shot grid 200x200m (b) horizon overlaid with five source points over the model.	32
Figure 3-14: 3D ray paths view at top of the model (a) smoothed 1D model (b) complex 1D model (c) complex 3D model (d) complex 3D model with Karst.	33
Figure 3-15: Hit count and offset ray maps for (a) smoothed 1D model (b) complex 1D model (c) complex 3D model (d) complex 3D model with Karst. The Hit count maps show illumination heterogeneities due to the overburden effect of the complex near surface.	34
Figure 3-16: Synthetic acoustic shot at offset 5km of (a) smooth 1D model (b) complex 1D model (c) complex 3D model (d) complex 3D model with Karst. Strong velocity inversion generates strong internal multiples and guided waves and Karst scatters the seismic energy.	35
Figure 3-17: synthetic shot in the middle of Arid model (a) acoustic wavefield (b) Elastic wavefield (c) Viscoelastic (d) Viscoelastic with multiples. Viscoelastic synthetic data with multiples are very correlate with real seismic data where dispersive ground roll, converted and shear waves are dominating the recorded land seismic data.	36
Figure 3-18: Interpretation of seismic wavefields (a) near-surface velocity model (b) viscoelastic synthetic shot overlaid with interpretation zones and horizons.	37
Figure 4-1: Data conditioning result, (a) raw shot gather, (b) shot gather after random noise attenuation (c) shot gathers after random & coherent noise attenuation (d) removed energies by noise attenuation application. Noise attenuation techniques suppress most of elastic and coherent noise and provide a better input to the acoustic FWI.	42
Figure 4-2: Stacked section with different constant velocities, starts from $V_p=1800$ -3400m/s every 400m/s increment as shown from (a) to (g), (h) shows values of optimum 1D stacking velocity and its stack at (i).	43
Figure 4-3: Manual velocity picking QCs and displays (a) semblance, (b) CMP gather, (c) multi-vel stack panels (d) Map shows velocity location every 500m, (e) table shows RMS velocity value of the current location and its interval and average (f) stack overlaid with interval velocity (g) stack overlaid with RMS velocity.	44
Figure 4-4: Surface wave inversion steps (a) windowing the surface wave energy (b) pick high semblance of its FK spectrum at all surface locations (c) a display of picks overlaid on semblance of all locations at certain frequency (d) V_s velocity inversion (e) stack shows good correlation between inverted velocity and Karst locations.	45
Figure 4-5: SWI provided more accurate velocity at top 200m (a) velocity from manual picking (b) velocity after SWI update.	46
Figure 4-6: RTM Global Image using initial model, (a) before SWI update, (b) after SWI update at bottom. SWI provides more accurate velocity at shallow part of the model which has a dramatic improvement on the subsurface image.	46
Figure 4-7: Shot gather input to FWI (a) early arrivals only (b) both refraction and reflection events. ...	47
Figure 4-8: Graph shows an example of the reduction of objective (misfit) function with inversion iterations at FWI 6Hz. The graph shows the reduction in misfit function starts to be stabilized from iteration 5.	48
Figure 4-9: Gradient conditioning (a) before conditioning (b) after conditioning. Gaussian smoothing filter helps to suppress the migration jittering and smiles at shallow part of the gradient.	50

Figure 4-10: Line search method (a) log_file of step length trail at 1 st iteration, (b) graph shows values of optimum alpha decrease with iterations.	51
Figure 4-11: Vp perturbations from different iterations at 6Hz FWI. The velocity change reduces with iteration as indication of stabilization in the objective function and the convergence.	51
Figure 4-12: P-velocity sections show that FWI can reconstruct accurately the karst velocity and low velocity layers (a) initial model (b) estimated FWI model (c) true model.	54
Figure 4-13:RTM Images of different velocity models (a) initial model (b) estimated model (c) true model. The subsurface RTM image comparison shows the similarity between the produced images using the true and estimated FWI models.	55
Figure 4-14: P-velocity sections of (a) initial model (b) estimated FWI model (c) true model, shows that acoustic FWI reconstructed successfully the small caves and karst geobodies and low velocity layers.	57
Figure 4-15: velocity profiles extracted at four different locations from the initial model (yellow line), estimated FWI model (red line) and true model (black line), show the similarity between the true and the estimated FWI velocity functions.	58
Figure 4-16: RTM Images of different velocity models (a) initial model (b) estimated model (c) true model. RTM iamges show a clear improvement of subsurface seismic image by using estimated FWI model.	59
Figure 4-17: RTM gathers of different velocity models (a) initial model (b) estimated FWI model (c) true model, show better flattening of the migrated gathers using the estimated FWI model relative to the migrated gather with the initial model.	59

LIST OF ABBREVIATIONS

NSM	:	Near-surface modeling
SEG	:	Society of Exploration Geophysicists
SEAM	:	SEG Advanced Modeling Corporation
FWI	:	Full Waveform Inversion
AFWI	:	Acoustic Waveform Inversion
RTM	:	Reverse Time Migration
KDM	:	Kirchhoff Depth Migration
SWI	:	Surface Wave Inversion

ABSTRACT

Full Name : Ali Ahmed Hussein Mohamed

Thesis Title : FULL WAVEFORM INVERSION FOR COMPLEX NEAR-SURFACE IMAGING USING SEG SEAM II SYNTHETIC MODEL

Major Field : Geophysics

Date of Degree : February 2018

Complexity in the Earth's near-surface zone introduces many challenges in land seismic exploration. In arid areas such as much of the Middle East, Karst features and unconsolidated sediments in the near-surface create velocity contrast, anisotropy and seismic energy attenuation that interfere with the imaging of deeper structure.

During the SEAM Phase II program, SEG and more than twenty Oil Companies constructed the Arid SEAM Phase II synthetic model as a realistic representation of strong geological heterogeneity of the arid desert areas of the Saudi Arabian.

In this thesis, I initially addressed the geophysical challenges of seismic wave propagation in the Arid SEAM model through finite difference forward modeling of acoustic to viscoelastic waves including multiples to enhance the understanding of features and artifacts in real seismic data. Then, I reviewed the theory of seismic wave inversion and the reverse time migration technologies to summarize the state-of-the art of depth and velocity imaging. Finally, acoustic FWI has been examined on two synthetic data created

using acoustic and viscoelastic forward modeling codes. For acoustic synthetic data, acoustic FWI successfully reconstructed velocity image with small local anomalies and strong velocity contrast. However, for the viscoelastic synthetic data with multiples, we applied seismic processing on the input data to eliminate all the waveforms that cannot be modeled by the acoustic engine, we also updated the very near-surface velocity using surface wave inversion which helped FWI to estimate the wavelet accurately from the first arrivals. This makes acoustic FWI work effectively and estimate accurate velocities for viscoelastic media and avoid the problem of cycle skipping, which leads to local minimum trapping and the wrong velocity model.

ملخص الرسالة

الاسم الكامل: على احمد حسين محمد

عنوان الرسالة: الانعكاس الموجي الكامل لتصوير التركيبات الارضية المعقدة القريبة من السطح باستخدام نموذج SEAM Arid SEG II الاصطناعي

التخصص: جيوفيزياء

تاريخ الدرجة العلمية: فبراير ٢٠١٨

يطرح التعقيد في منطقة الأرض القريبة من السطح العديد من التحديات في الاستكشاف الزلزالي للأرض. في المناطق القاحلة مثل الكثير من مناطق الشرق الأوسط حيث يوجد الفجوات و الرواسب وسط الصخور الأكثر صلابه في السطح القريب والتي تعمل على تباين السرعة وتوهين تباين الطاقة السيزميه و التي تتداخل مع تصوير بنية أعماق

اثناء المرحله الثانيه من برنامج سيمم قامت الجمعيه الجيوفيزياء الاستكشافيه بالتعاون مع أكثر من عشرين شركة بترول ببناء النموذج التركيبي كتمثيل واقعي للتغاير الجيولوجي القوي للمناطق الصحراوية القاحلة في المملكة السعوديه العربيه

في هذه الأطروحة ، تناولت في البداية التحديات الجيوفيزيائية لانتشار الموجات الزلزالية في نموذج خلال نمذجة الموجات الزلزالية من الموجات الصوتية إلى الموجات اللزجة لتعزيز فهم الميزات و الآثار في البيانات الزلزالية الحقيقية. بعد ذلك ، استعرضت نظرية انعكاس الموجة الزلزالية وتقنيات هجرة الوقت العكسي لتلخيص أحدث تقنيات تصوير العمق والسرعة. وأخيرا ، تم فحص الانعكاس الموجي الكامل على اثنين من البيانات الاصطناعية التي تم إنشاؤها باستخدام رموز النمذجة الصوتية. بالنسبة للبيانات الاصطناعية الصوتية ، نجح الانعكاس الموجي الكامل في إعادة بناء صورة السرعة مع حالات شاذة محلية صغيرة وتباين قوي في السرعة. و بالنسبة للبيانات التركيبية المرنة ذات المضاعفات ، طبقنا المعالجة الزلزالية على بيانات الإدخال للقضاء على جميع أشكال الموجات التي لا يمكن تصميمها بواسطة المحرك الصوتي ، وقمنا أيضًا بتحديث السرعة القريبة من السطح باستخدام انعكاس الموجة السطحية مما ساعد على تقدير الموجات بدقة من الوافدين الأول. وهذا جعل الانعكاس الموجي الكامل يعمل بشكل فعال ويقدر السرعات الدقيقة لوسائط اللزوجة ويتجنب مشكلة تخطي دورة ، مما يؤدي إلى الحد الأدنى من محاصرة المحلية ونموذج السرعة الخطأ

CHAPTER 1:

INTRODUCTION

Full waveform inversion (FWI) is a high-end earth model building tool in seismic industry which provides high resolution subsurface models from seismic data. Given a reasonable starting model, FWI is used to build accurate and detailed velocity models in marine environment, however it still has many challenges. In this chapter, we will briefly review reflection seismology, waveform inversion and the SEAM program. We discuss FWI challenges of land seismic data and summarize the thesis motivation and state its objective and methodology

1.1 Introduction

The growing challenges of land hydrocarbon exploration places an increasing demand on accurate, high resolution 3D seismic images to identify unconventional and low relief reservoirs with a small extension. Traditional geophysical tools for near-surface velocity reconstruction, such as refraction and diving wave tomography, are limited for cases with near-surface velocity inversion and strong lateral heterogeneity in the near surface.

FWI has been promoted as a tool to address such problems. It was initially proposed in the mid-1980s, this technology has become increasingly common in commercial applications due to increases in compute power. Over the last decade, the seismic industry has devoted

significant efforts to testing, developing and implementing FWI algorithms for building higher resolution velocity models which have helped to solve imaging problems such as pre-salt imaging.

In this work, I will begin with a conceptual review from the literature of FWI and the method on which it is based, seismic reverse time migration. I will summarize the definition of the complex near-surface problem and state the thesis objectives as well as the reasons for introducing FWI as a solution to characterizing the near-surface zone and removing its deleterious effect on deeper structure mapping.

The background and literature review in later sections give more details about hydrocarbon exploration in complex land environments, the Arid SEAM model as a realistic model for desert terrain environments, the theory of finite difference modeling and FWI plus the methodology and challenges of FWI.

1.2 Hydrocarbon exploration in complex land environments

According to current estimates, approximately $\frac{2}{3}$ of the remaining conventional oil and gas reserves in the world are located or will be found on land as shown in Figure 1-1 (https://en.wikipedia.org/wiki/Petroleum_industry). Furthermore, unconventional resources such as oil/gas shale and tight sands are playing an increasing role in the global energy supply (https://en.wikipedia.org/wiki/Oil_reserves).

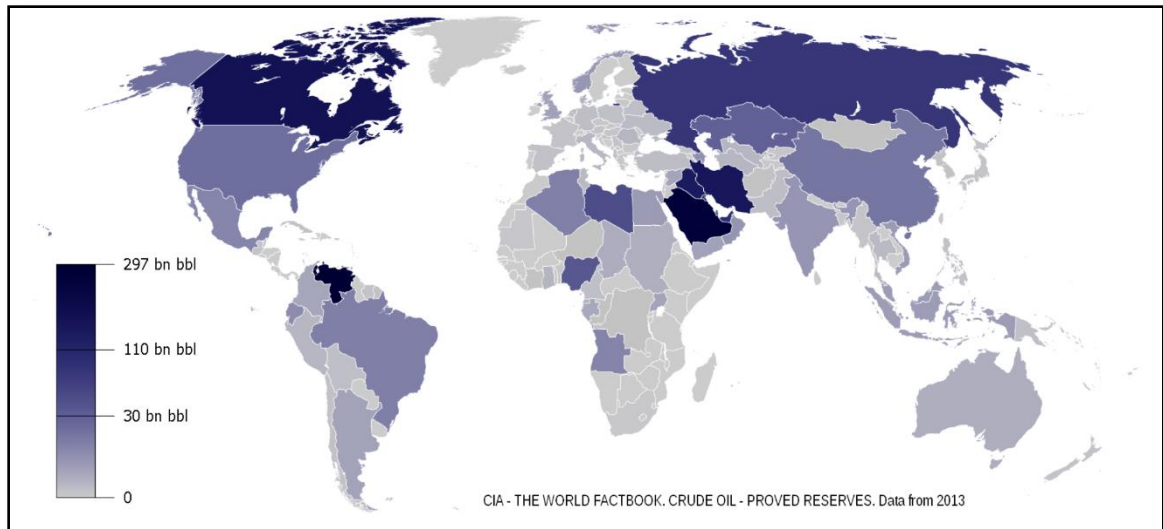


Figure 1-1: Map of world oil reserves in land, 2013. Darkness of the blue color indicates the amount of oil reserves.

However, many of these resources are found in environments where reflection seismology, a primary tool used for oil and gas exploration, is challenging due to near-surface complexity which masks deeper structure. This complexity has two dominant forms. In arid desert environments such as the Middle East and North Africa (shown in red in Figure 1-2 <http://caves.org/virtual/virtcave/Karst/Karst.html>), the presence of Karstic terrain and unconsolidated sands create extreme velocity contrasts and velocity reversals with depth. The complex geology found in fold and thrust belts such as Western America and Central Asia presents the second major challenge. Technologies that accurately image through such distorting features are critical to meeting our future energy needs.



Figure 1-2: Middle East and North Africa map with Karst regions (shown in magenta) where there are numerous oil exploration activities on land

Recognizing this challenge, 5 years ago the SEG launched the SEAM Phase II program to construct a synthetic 3D earth model on which algorithms could be tested to address land seismic exploration challenges. This model is described in the following section.

1.3 SEAM Program

In 2007, the Society of Exploration Geophysicists (SEG) started its partnership with oil companies to develop the SEAM program (SEG Advanced Modeling Corporation). This is a collaborative industrial research effort dedicated to large-scale, leading edge geophysical modeling and numerical simulation. The primary goal of SEAM is to advance applied

geophysical technologies on subsurface model construction and generation of synthetic seismic data sets to test algorithms for imaging and inversion, explore trade-offs in acquisition methodologies and enhance understanding of features and artifacts in real seismic images.

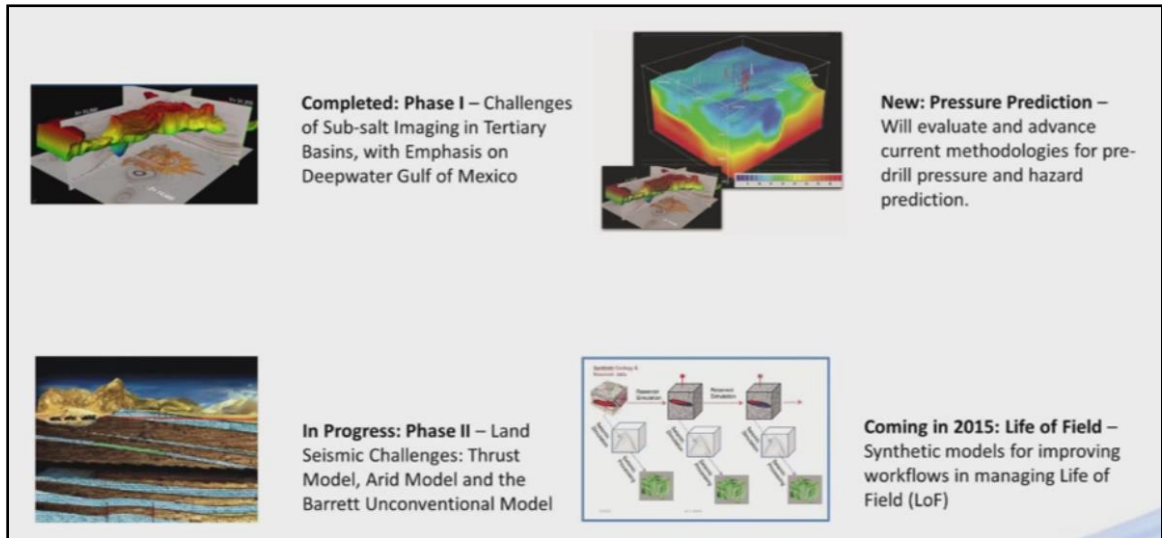


Figure 1-3: Past, present and future SEAM models, presented at SEG October 2014, Phase I represents challenges of sub-salt imaging, Phase II shows land seismic challenges, the objective of Phase III is to advance current methodologies of predrilling pressure and hazards predictions and Phase IV is used to improve the workflows in managing the life of the field.

In 2011, SEG launched SEAM Phase II under the theme of “Land seismic challenges” with sponsorship of 22 oil companies to construct models having a realistic representation of land seismic challenges, from dealing with near-surface heterogeneity at scale of meters to kilometers, to incorporating full elastic seismic wave propagation. SEAM Phase II consists of three models: The Foothills model with very rough topography representing mountain thrust zones; the Barrett model representing two types of unconventional reservoirs

based on Eagle Ford and Woodford shale plays; and the Arid desert model that will be used in our study and will be discussed in more detail in the literature review section below.

1.4 Reflection seismology

Reflection seismology is a method of exploration geophysics that uses the travel times and amplitudes of reflected seismic waves from controlled sources (e.g., explosions, vibrators, air-gun...etc.) to estimate the properties of the Earth's subsurface. It is the primary tool used in oil and gas exploration and reservoir monitoring. Waveform data from these measurements are typically migrated and stacked (after appropriate pre-processing) to form an image of the sub-surface, or may be inverted using iterative algorithms to recover an earth property model. With suitable processing and interpretation, reflection seismology can yield information on both the structural and the pore fluid properties of the subsurface geology (https://en.wikipedia.org/wiki/Reflection_seismology).

A great deal of research has been devoted to techniques for processing seismic data in order to resolve near-surface complexity. Examples of such techniques include FWI and simultaneous joint inversion using seismic and potential field data or first arrival P-wave with surface wave data. FWI was proposed

by Tarantola in 1984. It has grown in popularity in recent years as computer power has increased to solve the complex waveform propagation equations in FWI and RTM. The latter primarily recovers the geometry of the reflectors and it requires a good macro-velocity model, such as from FWI. However, the applicability and resolving power of FWI in different environments is still being explored. As it is generally not possible to fully assess the accuracy of an earth model obtained from real data, such studies are best approached using synthetic models.

1.5 Thesis Objectives

The primary objective of this thesis, is to more effectively characterize the near-surface zone using FWI in both its theoretical and practical components. I will study the behavior of seismic wavefield for a complex near-surface areas having geological heterogeneities and its impact on seismic wave propagation and subsurface imaging. I will examine if Full Waveform Inversion can accurately reconstruct suitable models of small shallow geological features

with strong velocity contrast, resulting in improved seismic subsurface imaging.

1.6 Thesis overview and contributions

This thesis report contains five chapters. The current and first chapter gives an overview of reflection seismology, FWI and the challenges of seismic imaging in land environment with a complex near surface. In the second chapter, we give more details about the theory of finite difference modeling and FWI methods and the cycle skipping problem along with the strategy used to overcome this issue. We demonstrate in chapter 3 the geological features that are present in the SEAM Phase II Arid model as a realistic representation of the Arabian Peninsula geology then we evaluate the effect of such complex geological features on seismic waves and their imaging through finite difference modeling. Chapter 4 contains a FWI workflow and how we determine the starting model and preparation of the input data to avoid being trapped in local minima. Finally, we present the result of the FWI on two different synthetic data sets; the first is acoustic and the second is viscoelastic with multiples and noise included. Chapter 5 contains an overall summary of this report along with a discussion and our conclusions.

CHAPTER 2:

FWI: Theory, methodology and technical description

The objective of this chapter is to introduce the numerical modeling methods, especially the finite difference technique, then we discuss FWI theory, methodology and technical description of its main steps and cycle skipping problem as the main challenge of FWI.

2.1 Numerical modeling

Most geophysical algorithms rely on some form of using numerical modeling. There are two types of numerical modeling to consider: forward modeling which generates synthetic data using a parameterized representation of the subsurface and inverse modeling which inverts the measured or observed data to predict the model parameters as shown in Figure 2-1.

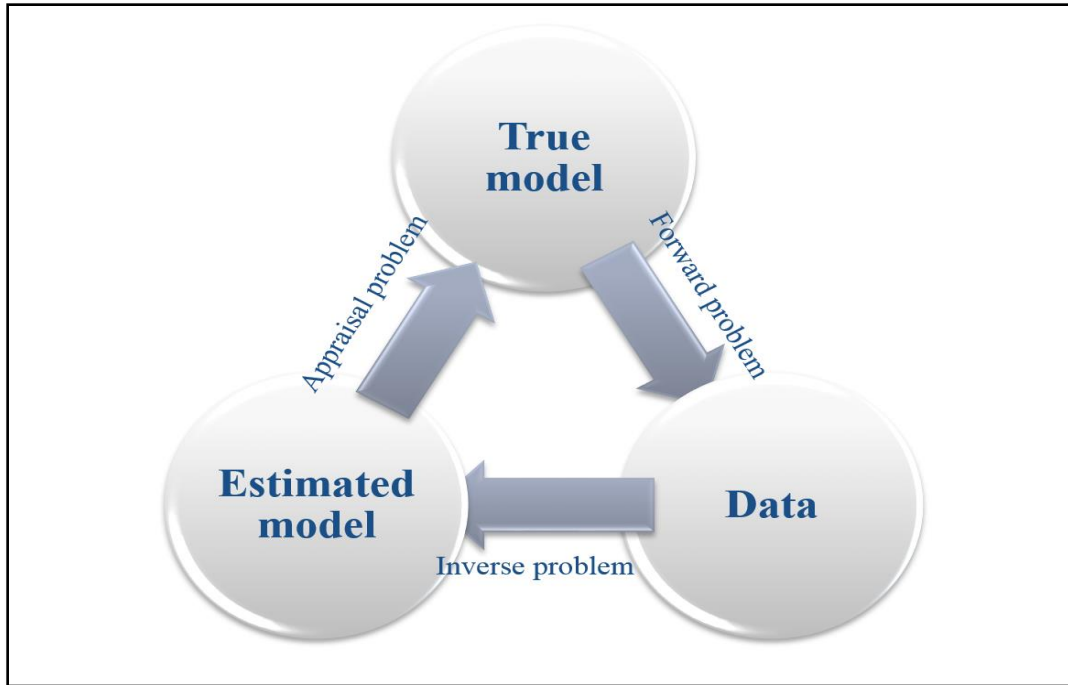


Figure 2-1: A schematic chart shows the relation between forward, inverse and appraisal problems.

Numerical modeling is widely used to tackle a complex geophysical problem by computational simulation of geophysical scenarios, so it has significant importance and applications in seismic exploration, for instance survey design and modeling, seismic processing, imaging and interpretation.

Many numerical methods are available for implementing forward modeling for example the finite difference method, the pseudo spectral method, finite element method, the spectral element method, the boundary integral method and various hybrid schemes.

2.2 Finite difference forward modeling

The finite difference method (Robertson, 1996) is extensively used in seismic wave propagation simulation because it is powerful and easy to be implement in a modeling code. It approximates the governing differential equations with their discretized

equivalents by replacing the partial derivatives with a finite difference estimation based on a truncated Taylor series expansion.

For the illustration of the basic theory of finite difference method for 2D acoustic wave equation in a medium with constant density:

$$c(x, z)^2 \left[\frac{\partial^2 p}{\partial x^2}(x, z, t) + \frac{\partial^2 p}{\partial z^2}(x, z, t) \right] - \frac{\partial^2 p}{\partial t^2}(x, z, t) = s(x, z, t) \quad (1)$$

Equation (1) is the derivative form of the 2D acoustic wave equation in a medium with constant density where $p(x, z, t)$ is the pressure field, $c(x, z)$ is the velocity field and $s(x, z, t)$ is the source wavelet for the implicit line source in the y direction.

By using the general form of the finite difference solution for the 2nd partial derivatives of $f(x, z, t)$:

$$\frac{\partial^2 f}{\partial x^2}(x, z, t) \cong \frac{f(x-\Delta x, z, t) - 2f(x, z, t) + f(x+\Delta x, z, t)}{\Delta x^2} \quad (2a)$$

$$\frac{\partial^2 f}{\partial z^2}(x, z, t) \cong \frac{f(x, z-\Delta z, t) - 2f(x, z, t) + f(x, z+\Delta z, t)}{\Delta z^2} \quad (2b)$$

$$\frac{\partial^2 f}{\partial t^2}(x, z, t) \cong \frac{f(x, z, t-\Delta t) - 2f(x, z, t) + f(x, z, t+\Delta t)}{\Delta t^2} \quad (2c)$$

We can define the finite difference equation of the 2D acoustic wave equation in a medium with constant density by substituting equations (2) into (1), which yields

$$\begin{aligned}
p(x, z, t + \Delta t) = & r^2[p(x - \Delta x, z, t) - 2p(x, z, t) + p(x + \Delta x, z, t)] + \\
& r^2[p(x, z - \Delta z, t) - 2p(x, z, t) + p(x, z + \Delta z, t)] - p(x, z, t - \Delta t) + \\
& 2p(x, z, t) - \Delta x^2 r^2 S(x, z, t)
\end{aligned} \tag{3}$$

where $r = c\left(\frac{\Delta t}{\Delta x}\right) = c\left(\frac{\Delta t}{\Delta z}\right)$ and $\Delta x = \Delta z$ and Δt are the space and time sample intervals.

The time step and cell size should be carefully defined to avoid instability and dispersion in the modeling results. For 4th order spatial derivatives the Courant number is 0.606 (Sei, 1995) and for stability the discretization must satisfy; $c \frac{\Delta t}{\Delta x} \leq 0.606$ this approximately requires that $\Delta t < \frac{0.606\Delta x}{c_{max}}$ to have stable modeling results where $\Delta x = \Delta z$ is the discretization step in the spatial dimensions. Dispersion for the 2D wave-equation will occur more strongly and clearly visible if the following relation is not obeyed

$$\Delta x = \Delta z < \frac{c_{min}}{5f_{max}} \left(= \frac{\lambda_{min}}{5} \right)$$

To simulate seismic wavefield of 2D isotropic acoustic medium with constant density using equation (3), we need a velocity model, source wavelet and define the optimum value of $\Delta x = \Delta z$ and Δt to avoid instability and dispersion in the modeling result.

In the first step of the FWI workflow, we perform forward modeling of the data by wavefield extrapolation of the source wavelet using a finite-difference method to numerically solve the two-way wave equation.

2.3 FWI theory

Seismic (full) waveform inversion (e.g. Tarantola, 1984, 1986; Mora, 1987; Crase et al., 1990; Sears et al., 2008) attempts to reconstruct a subsurface model that best explains the observed data in a least-squares fitting sense such that the difference between the actual data and that computed (predicted) for the model is minimized. Although using all the data for model building sounds attractive, the inversion itself is plagued by non-linearity issues which become acute if the velocity contrasts are large and the starting model is not close to the true (unknown) model.

An incorrect model may provide a reasonable data fit to the data but the iterative optimization procedure cannot move away from this model as the algorithm gets trapped in a local minimum of the objective function (Mulder and Plessix, 2008). Factors that contribute to the challenge of applying Full Waveform Inversion to land data include variations in source and receiver coupling, strong near-surface effects such as attenuation, ground roll, and scattering due to rapid geological variations and topography. Elastic inversion in such a setting, when only the usual single component data without low frequencies are available, remains a formidable problem for the time being, not only because of the ill-posed nature of determining density, velocity and attenuation of P- and S-waves, and anisotropy all at the same time, but also because of the computational cost of modeling waves with very small S-velocities. (Mulder & Perkins, 2010). Instead, we currently take the more common approach of improving the velocity model by using the acoustic approximation (Operto et al., 2004; Brenders and Pratt, 2007) starting with the

lowest frequencies and filling in more details by gradually increasing the bandwidth of the data.

2.4 FWI flowchart and methodology

Time domain acoustic FWI workflow using multi-scale approach and later damping strategy has been implemented in this project to update the P-wave velocity on two different datasets acoustic and viscoelastic with free surface multiples and noise. The results will be discussed in chapter4.

In Figure 2-2, I explain the acoustic FWI flow which I propose to use to reconstruct the final velocity model.

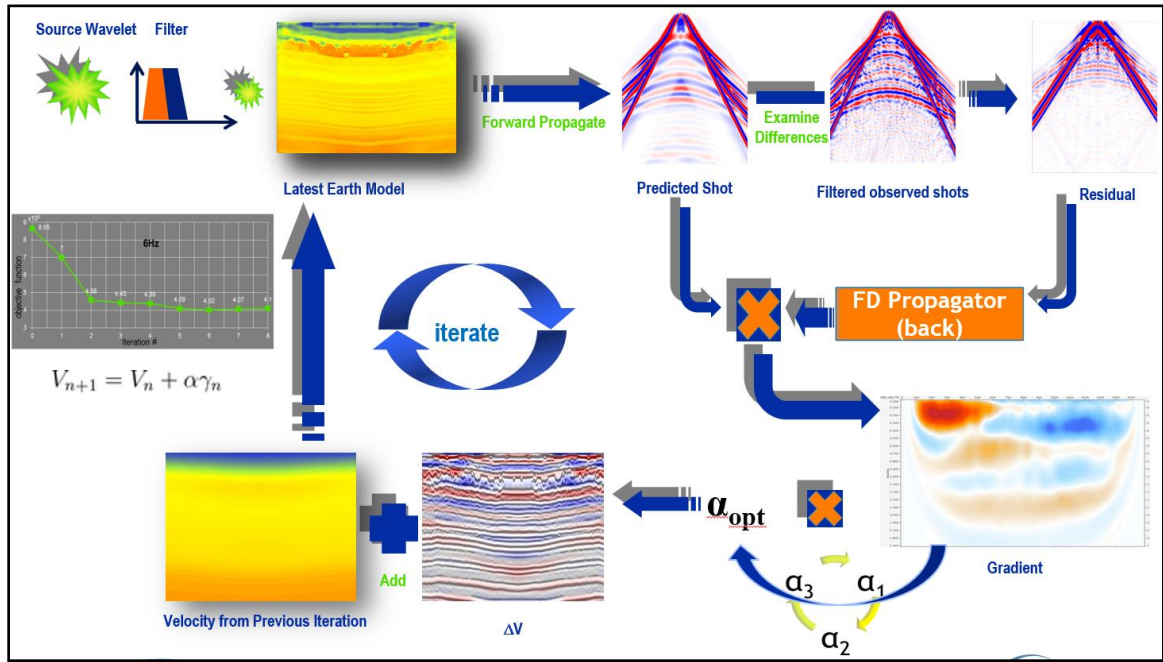


Figure 2-2: Multi-scale time domain acoustic FWI flowchart. This flow updates the primary velocity by minimizing the difference between predicted and observed data through an iterative process which starts from low frequency and progressively increases the bandwidth of the data.

The steps in this flowchart are as follows:

- 1 Define the starting frequency band then filter the source wavelet and input seismic data equivalent to starting frequency band
- 2 Simulate seismic data with the starting velocity model or the updated velocity model for each subsequent iteration. The simulation is carried out using a time-domain finite-difference solution to the acoustic wave equation (Vigh and Starr, 2009)

$$\frac{1}{c(x,z)^2} \frac{1}{\rho} \frac{\partial^2 p}{\partial t^2} = \left[\frac{\partial}{\partial x} \left(\frac{1}{\rho} \frac{\partial p}{\partial x} \right) + \frac{\partial}{\partial z} \left(\frac{1}{\rho} \frac{\partial p}{\partial z} \right) \right] + s(x, z, t) \quad (4)$$

where $p(x, z, t)$ is the pressure field at position x, z as function of time t , $c(x, z)$ is the spatially variable velocity field, $\rho(x, z)$ is the density and S is the source wavelet.

- 3 Calculate the misfit function between the observed pressure field $p_{obs}(x, z, t)$ and the predicted pressure field $p_{cal}(x, z, t)$ which is calculated in step 2 (Vigh and Starr, 2009)

$$E = \frac{1}{2} \sum_s \sum_r \int dt [p_{cal}(x, z, t) - p_{obs}(x, z, t)]^2 \quad (5)$$

- 4 Minimize E iteratively by calculating the gradient or steepest-descent direction (Tarantola, 1984) at iteration n by

$$\gamma_n = \frac{1}{c_n^3} \sum_s \int \partial t (\partial_t P_f) (\partial_t P_b) \quad (6)$$

where $P_f(x, s|t)$ is the forward-propagated source wavefield, and $P_b(x, s|t)$ is the back-propagated residual wavefield into the model using the misfits ($P_b = P_{obs} - P_{cal}$) acting as if they were sources at the receiver locations. Both wavefields are propagated using the current velocity and density fields.

- 5 Update the velocity using

$$c_{n+1} = c_n + \alpha \gamma_n \quad (7)$$

where α is the step length. The step length may be a linear estimate or using line search methods (Vigh and Starr, 2009).

- 6 Move to higher frequency band and repeat the above-mentioned steps until reach the desired resolution of the velocity update

2.5 FWI technical description

FWI updates the velocity model by minimizing the difference between observed (recorded) and synthetic (modeled) seismic data. The synthetic seismic data is modeled using the starting velocity model. In this process, the first step is to generate accurate modeled data which is done by numerically solving the acoustic or visco-acoustic two-way wave equation using finite difference methods. In the modeling process, a model of the density is needed as well as a good estimate of the source wavelet in the data.

The second step, the velocity model update, can be obtained by minimizing the travel time difference between modeled and observed data and/or by minimizing the amplitude differences between modeled and observed data.

2.5.1 Forward modeling of the data

In forward modeling, we are simulating the observed data as closely as possible, hence the source wavelet is very important. The best choice for the source wavelet required for the forward modeling is to extract it from the data. In case of performing acoustic FWI, the initial earth model should contain both P-velocity and density models.

Acoustic forward modeling simulates all P-wave energy such as reflection, internal multiple, guided wave but the free surface multiple can be excluded by applying an absorbing boundary at the top of the model. Forward modeling includes geometrical spreading of the wavefront and transmission losses effects. Any random and coherent noise, shear and surface waves in real data should be attenuated before acoustic FWI because they are not included in the forward modeling.

The velocity model update can be inverted for by

- Minimizing the travel time difference between modeled and observed data
- Minimizing the least-squares waveform differences between modeled and observed data.

2.5.2 Residual using least square objective function

It is waveform differences between the observed and the predicted data. The residuals contain all the events in the data including direct arrivals, water bottom reflections, refracted and reflected events and multiples. In addition, it will contain any random or coherent noise that was left in the observed data. We might want to exclude some of the seismic events before the inversion based on the FWI strategy.

2.5.3 Travel time errors using travel time objective function

An alternative measure for the difference between observed and modeled data is the travel time difference between the same events on the two datasets which can be inverted to give velocity gradient of the updates. The waveform inversion using residuals is more vulnerable to cycle skipping problem than travel time error.

2.5.4 Cycle skipping and local minimum trapping

Cycle skipping occurs when the time shift between the observed and modeled data is larger than half a cycle of the typical wavelet which makes FWI update in the wrong direction, thus converging into local minimum and not the global minimum. As the cycle time depends on the typical frequency in the wavelet, cycle skipping increases with increasing frequency. A low frequency wavelet is far more tolerant of a kinematic time discrepancy since it would be a much lower fraction of the wave period. Some strategies have been proposed to overcome this issue as multiscale strategy and damping later arrivals.

The idea of a multiscale strategy is to invert for long wavelength (low spatial frequency) velocity variations first and progressively move to short wavelengths to update small details in the velocity model as iterations proceed. This is illustrated by Bunks et al. (1995)

The late arrivals are often dominated by reflections and multiples which have more local minima than early arrivals, as shown by Sheng et al. (2006). This above strategy is proposed by Pratt and Worthington (1988)

Both strategies have been utilized during this project where I initially invert refraction energy (early arrivals) only at low frequency then progressively including reflection at higher frequency.

2.5.5 Velocity gradient and model update

The inversion process is designed to minimize the residuals or travel time errors in a least squares sense which has two steps

1. Calculating the objective function gradient = direction of the update

2. Determining a scalar for the optimum velocity update along this direction using a line search technique (Hager et al, 2005)

First, the residuals are backward propagated into the depth model and a zero-lag cross-correlation with the forward propagated wavefield (for a specified source signal) is carried out to give the gradient. This gives the direction and relative magnitude of the updates but not the absolute velocity model update values. A line search is then performed where the residuals are calculated for a small number of velocity gradient scalars. The misfit functions are computed for the small number of trial scalars then the optimum step length is defined through a parabolic fitting of the misfit functions plot. The model update is determined by scaling the objective function gradient by optimum step length then added to pervious model to get a new model. |

|

CHAPTER 3:

Seismic wave propagation in the complex near surface

In this chapter, we discuss the geological features exist in Arid SEAM model and their realistic representation of arid environment in the Arabian Peninsula, then we address the effect of such complex near-surface geology on seismic wave propagation by means of an asymptotic ray tracing method and a finite difference forward modeling method.

3.1 Near-surface geology of Arabian Peninsula

The Arabian Shelf platform is built up by sedimentary sequences of Paleozoic to Cenozoic rocks. These sequences surround the shield area in the west and dip slightly towards the east and northeast below the over thrust of the Zagros Mountains (Powers et al, 1966; Chapman in Al-Sayari & Zoetl, 1978).

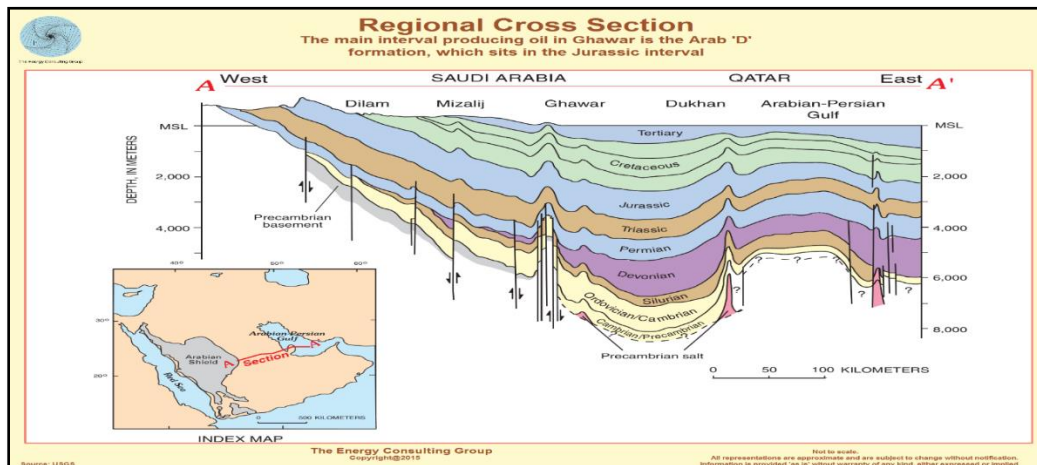


Figure 3-1: Regional geological cross section from west to east of Saudi Arabia (Courtesy of USGS), shows the thickness of the sedimentary rock increases from west to east of Saudi Arabia.

The Paleocene to lower Eocene UER formation outcrops about 70 to 150 km east of Riyadh in a relatively narrow (50 km) but very extensive slightly curved belt, which can be

followed from the Rhub al Khali in the south to the Iraq-Saudi border over more than 1000 km (Bramkamp & Ramirez, 1958) as shown in Figure 3-1. The sequence consists of fossiliferous fine-grained recrystallized limestones with intercalated calcarenites and dolomites. They are underlain by Cretaceous marls and dolomites of the Aruma formation and superposed to the east by sandstones and marls of the Miocene. The superposition of the Miocene marks an important erosion unconformity.

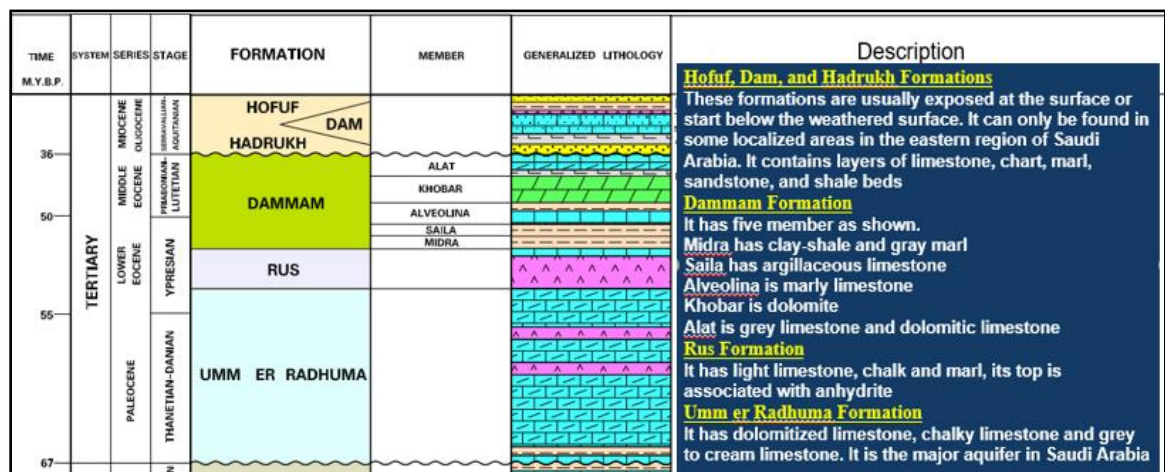


Figure 3-2: Geological stratigraphic column of the Tertiary rocks at eastern of Saudi Arabia (Courtesy of LUKSAR), Tertiary system consist of six main formation which introduces strong velocity contrast due to the intercalation between low velocity (sand and shale) layers and fast velocity (anhydrite, dolomite and limestone) layers.

Figure 3-2 shows a summary of the Saudi Arabian stratigraphic column of the Tertiary system which consist of three main formations of Paleocene to Eocene age from bottom to top, Umm er Raduma, Rus and Dammam formations, superposed by Miocene -Oligocene formations which are Hadruk, Dam and Hofof. The generalized lithology is described at the same Figure for each formation where the UER formations are mainly dolomitized limestone, chalk limestone and grey to cream limestone. It is a major aquifer in the eastern part of Saudi Arabia. After the deposition of the UER formation the sea drew back towards the Gulf, where thick marls and evaporites (Rus Formation) and limestones (Dammam Formation) were deposited during the Eocene. The western part of the UER became land

and was exposed to strong Karstification (Hoetzi et al., 1993). Its later sedimentary cover was produced mainly by terrestrial accumulation processes during the Miocene. Since the upper Miocene has been developed under prevailing arid climatic conditions and repeatedly intercalated short wet (semiarid) phases with erosion processes.

In the next section, we demonstrate that the SEAM Phase II Arid synthetic model is a realistic representation of the Tertiary rock system of the eastern part of Saudi Arabia

3.2 SEG SEAM Phase II Arid synthetic model

The Arid SEAM Phase II model exhibits the same reservoir and stratigraphy as the unconventional SEAM (Barret) model, but replaces the first 500 meters with complex near-surface features encountered in desert terrains like the Arabian Peninsula. In such terrains, features including Karst, wadis, stream channels and low-velocity unconsolidated sediments in the near-surface introduce strong velocity contrasts that generate extreme near-surface signal scattering often seen in seismic records from arid terrains.

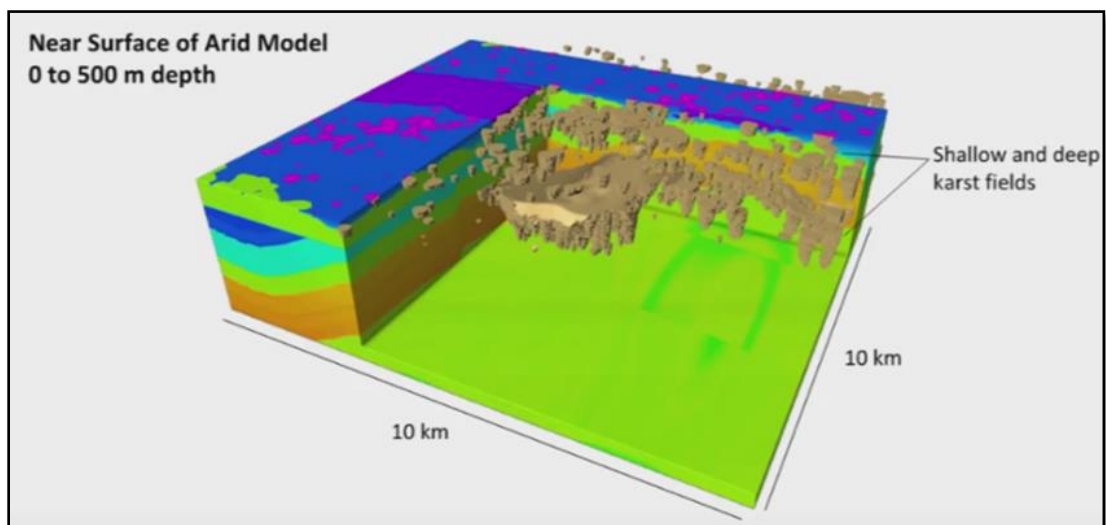


Figure 3-3: Near-surface of arid model with shallow and deep Karst fields (SEG.org) shows complex velocity variation due to the presence of low velocity karst geobodies and unconsolidated sediment within the bed rock.

The Arid Model is 10 km \times 10 km in horizontal extent and 3.75 km in depth. It is discretized into uniform 6.25-m blocks. Figure 3-3 shows a perspective view of the first 500 m of the model as seen from its northwestern corner. The near-surface zone consists of a series of tilted quasi-parallel layers representing hard bedrock, which is cut by a buried erosional surface, filled with a hard alluvium (red), and planed off at the top to simplify numerical simulations of the free-surface boundary condition at the earth-air interface.

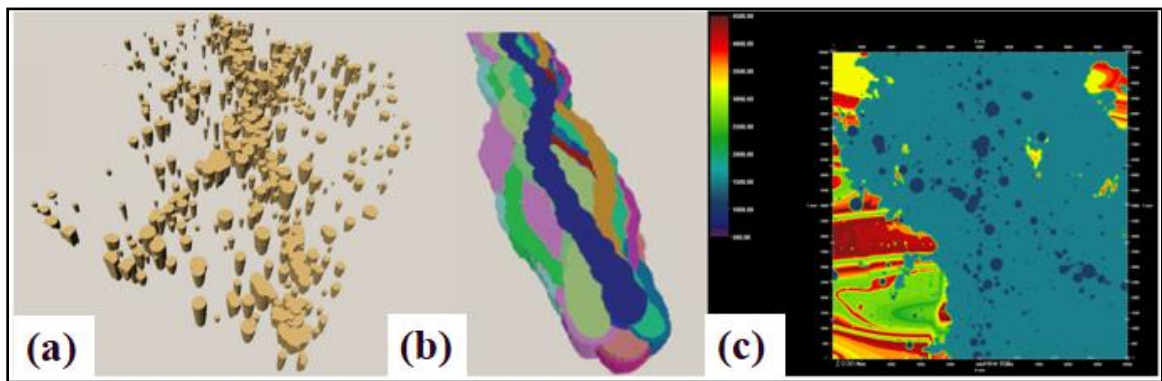


Figure 3-4: Geological features at top of Arid (a) 3D structural modeling of shallow Karst fill with very slow materials (b) Wadis and buried rivers bed (c) Depth slice of top of the velocity model shows strong velocity heterogeneities (Displays courtesy of Schlumberger WesternGeco. Source is SEG.org).

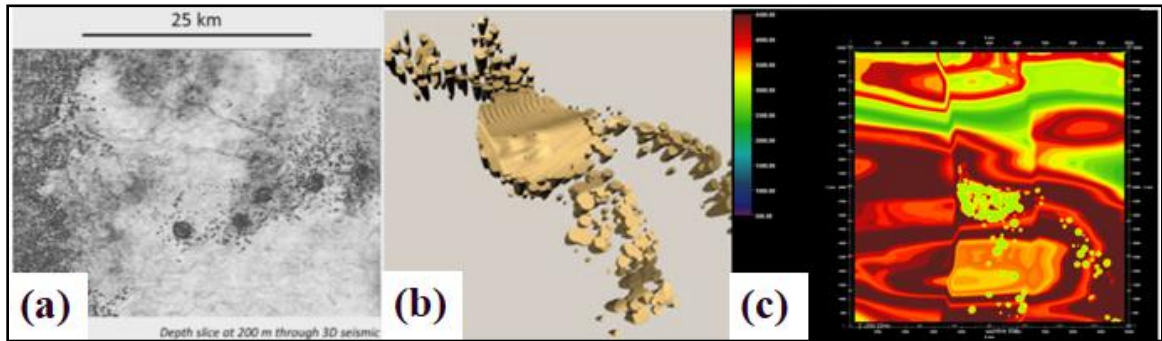


Figure 3-5: Geological features at 200m of Arid model (a) depth slice at 200m through 3D real seismic (b) 3D structural modeling of deeper Karst (c) Depth slice at 200m in the velocity model (Displays courtesy of Schlumberger WesternGeco. Source is SEG.org).

The bedrock outcrops sporadically along the western edge of the model. The interior of the model contains shallow and deep Karst fields. Karst refers to cavernous limestone in the subsurface formed by acidic rainwater that dissolves carbonate bedrock as it percolates

down from the surface. The cavities are filled with unconsolidated sands having very low-velocity 700-1000m/s which produces a situation of large contrasts in seismic velocity as shown in Figures 3-4 and 3-5.

Further information about the SEAM Arid model can be found on <https://seg.org/News-Resources/SEG-Advanced-Modeling-SEAM/SEAM-Projects/Phase-II-Land>.

In the last two sections, we demonstrate that the Arid SEAM Phase II synthetic model is representing a complex near-surface with small geological heterogeneities that are exhibited in the Arabian Peninsula.

3.3 Finite difference modeling using FDelmodc software

The modeling package used, FDelmodc, is an open source software which makes use of the Seismic Unix interface to read model parameters, source and receiver geometry files and produces the output files with SU-segy header format. The program can model seismic waves conforming to the 2D wave equation in different media which allows the implementation of four different finite difference schemes: acoustic, elastic, viso-acoustic and viscoelastic without/with free surface multiples.

3.4 Source wavelet generation

As an advantage of FDelmodc, which uses input in SU format, I used MAKEWAVE su command to generate the source wavelet as input to finite difference modeling. This wavelet is a Klauder wavelet which is like a Vibroseis sweep after the auto-correlation process, which is the practice in land seismic acquisition.

Figure 3-6 shows the Makewave command used to create the source wavelet of time length =1 second, and temporal sample interval is 0.8 millisecond. This wavelet has a flat amplitude spectrum from 3-20Hz and a zero phase spectrum. The maximum frequency of this wavelet is limited to 20Hz due to the limited available computer resources during the project lifetime, especially the computational cost of viscoelastic modeling which increases exponentially with increasing frequency.

This wavelet has been used to generate viscoelastic synthetic data with free surface multiples and random noise as input to the FWI work.

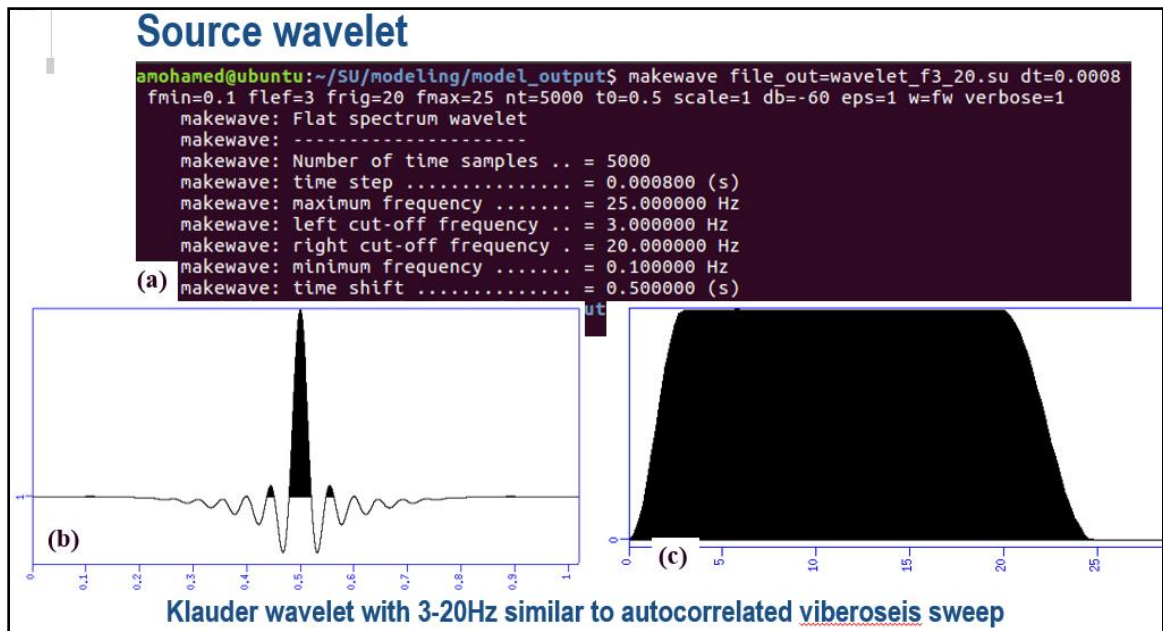


Figure 3-6: Klauder wavelet with zero phase spectrum generated (a) Makewave command in su and wavelet attributes (b) the wavelet in time domain (c) amplitude spectrum shows flat spectrum from 3-20Hz.

3.5 2D line extraction and expansion from SEAM model's parameters

FDelmodc software is limited to 2D wave-equation modeling, so we extracted along 2D lines all the arid model parameters (V_p , V_s , density, Q_p and Q_s). This 2D line is selected to cross most of the complex geological features represented in the 3D model as shown in Figure3-8 as the solid white line.

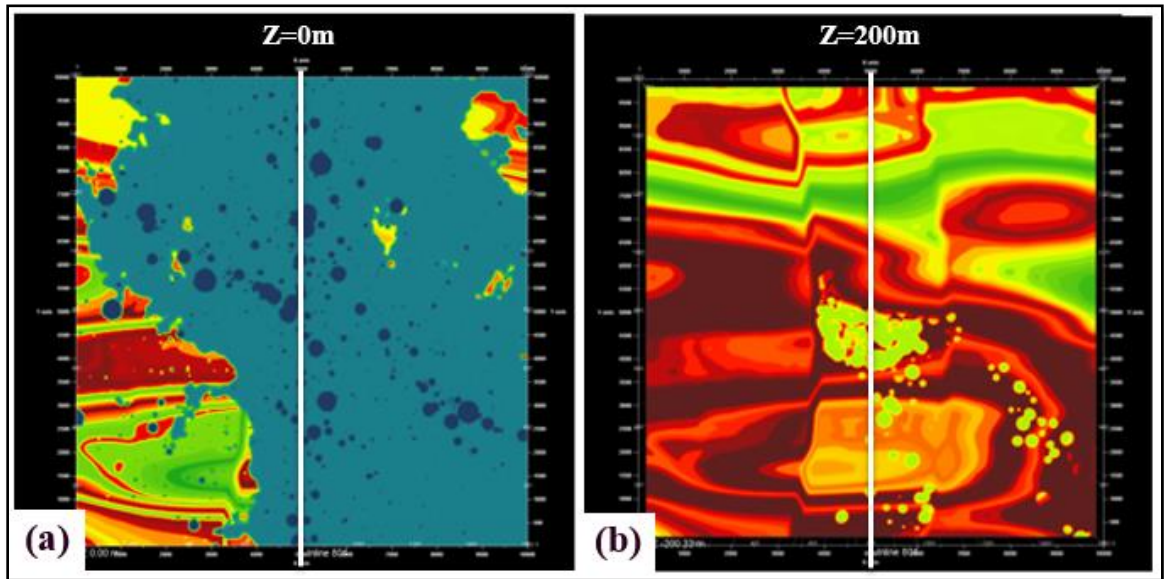


Figure 3-7: 2D line is shown as white solid line over V_p Arid model (a) depth slice at top of the model (b) depth slice at 200m in the model.

Figure 3-7 shows the selected line crossing at the top of the model through caves filled with unconsolidated clastic material and a depth slice at 200m shows this line passing through groups of Karst limestone of $V_p=5000\text{m/s}$ filled with clastic sedimentary rock $V_p=2200\text{m/s}$.

Afterward, we expanded the 10km 2D line to 20km length by mirror imaging it as shown in Figure 3-8, which helps to increase the model usability and to evaluate the outcome results over the full inverted and imaged area.

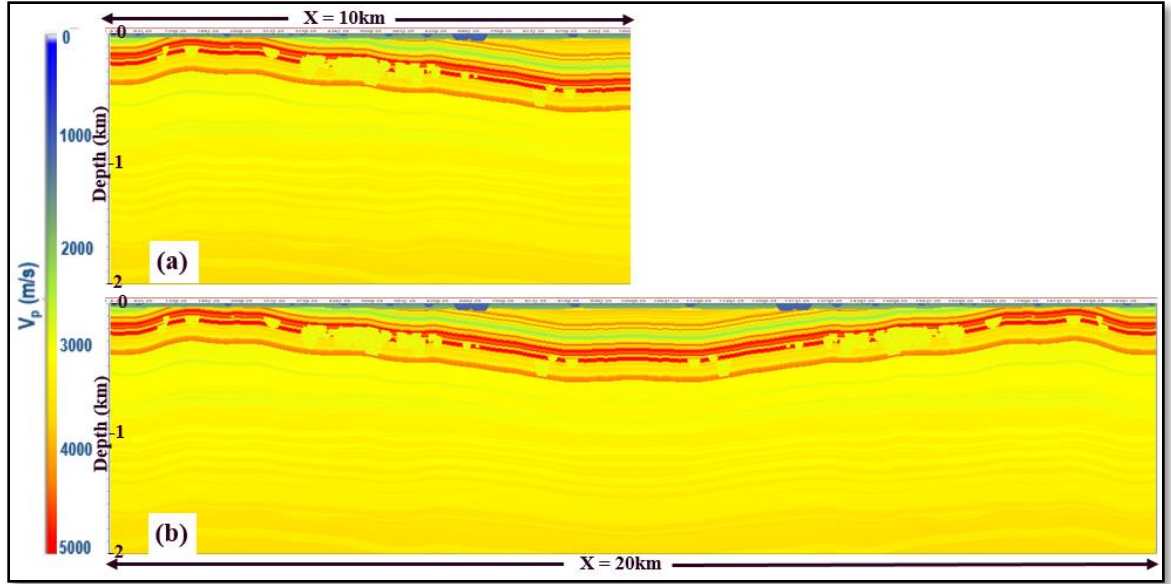


Figure 3-8: 2D Vp model (a) Original Vp with 10km length (b) Extended Vp with 20km length.

Four models have been extracted and extended as shown in Figure 3-9, I used these models as the input to the forward modeling experiment and to the simulation of the synthetic data for the FWI experiment.

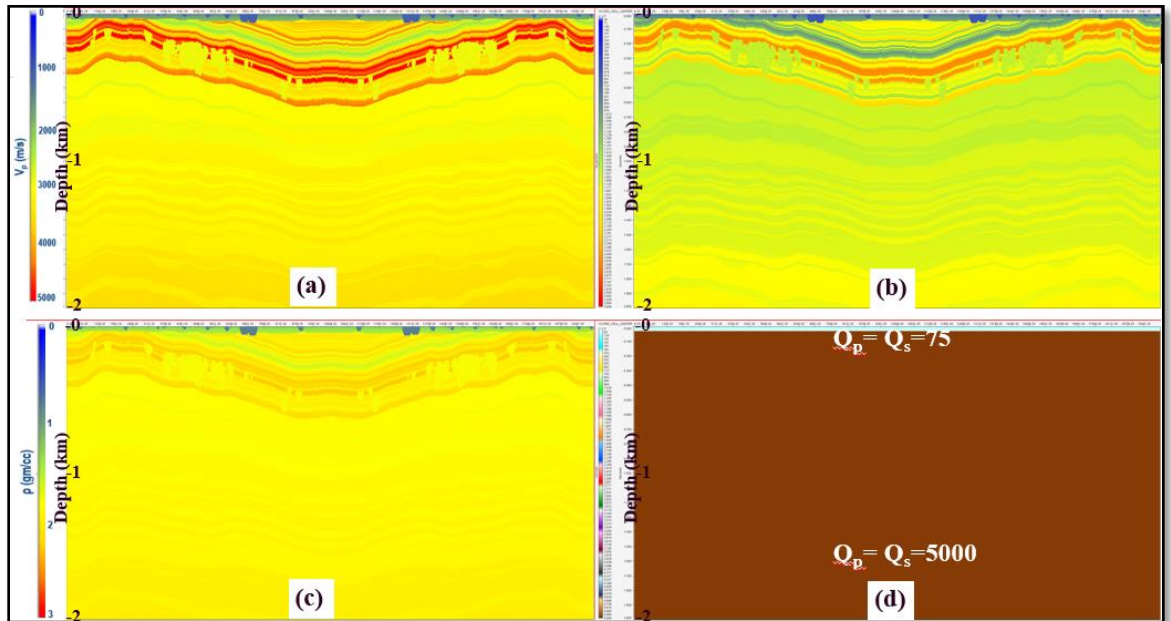


Figure 3-9: Arid SEAM model properties, (a) Vp, (b) Vs, (c) rock density and (d) $Q_p=Q_s$.

3.6 Ways of addressing complex near-surface geology through ray tracing and finite difference modeling

One of the objectives of creating synthetic models is to have a better understanding the features and artifacts in real seismic data. To examine the effect of strong heterogeneity on the full seismic wavefield, we use both the ray tracing method and the finite difference forward modeling to simulate the full wavefield progressively starting from acoustic to viscoelastic with multiples. To achieve this, we decompose the complexity of the Arid SEAM model into three simpler models with the aim to understand the effect of strong velocity inversion and Karst separately.

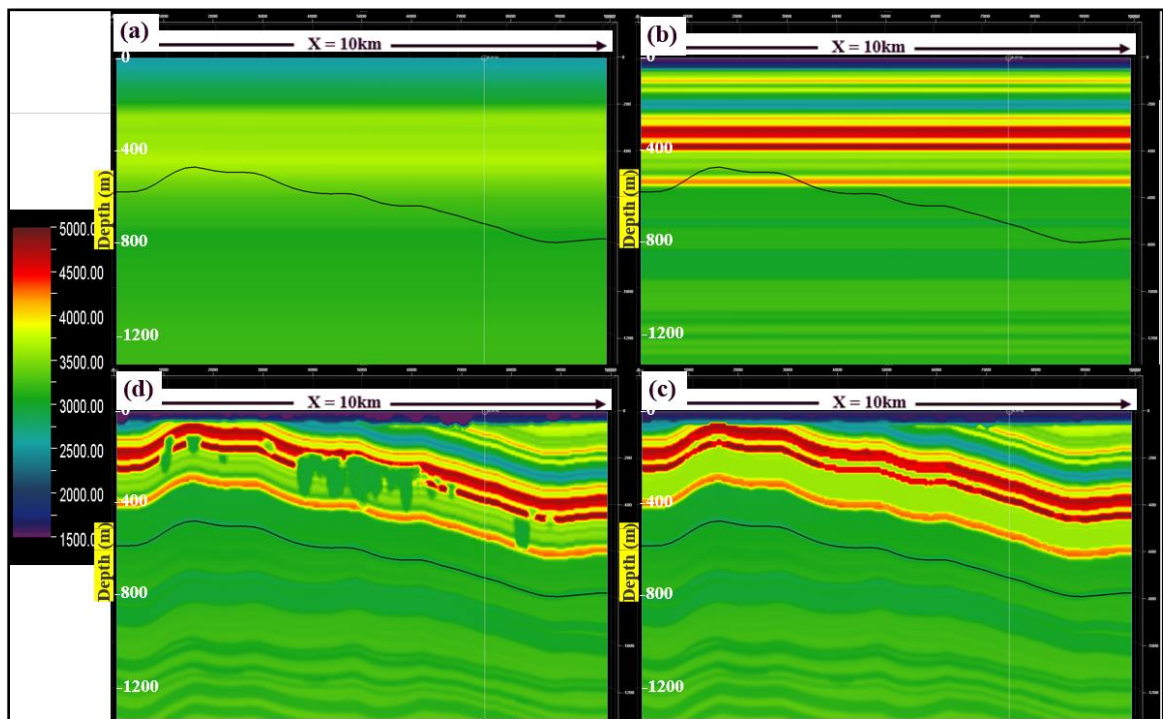


Figure 3-10: Four velocity models represent different levels of near-surface complex geology (a) smooth velocity variation (b) strong vertical velocity variation (c) strong spatial and vertical velocity variation (d) Arid SEAM model that has a complex velocity variation including Karst with slow velocity.

Figure 3-10 shows four different models where the degree of complexity increase from 3-10a to 3-10d. Figure 3-10a is the simplest model with gentle trend of the 1D velocity, Figure 3-10b represents a 1D model with pronounced vertical velocity inversions, whereas Figure 3-10c shows a 3D complex velocity model like the arid SEAM model but without Karst and the last model is the arid SEAM model as shown in Figure 3-10d.

We used two seismic modeling methods, the ray tracing method and the finite difference method to examine the behavior of seismic wave propagation in these four models.

3.6.1 Ray tracing method

Ray tracing methods are frequently used in seismic modeling and imaging, where the seismic wavefield is represented as a series of specific events (e.g., reflections) with characteristic travel time and amplitude. We created an interface based 2D model from Arid SEAM 3D gridded model by digitizing it into layers having piecewise constant velocity and density. The ray paths are reflected and transmitted at velocity interfaces only according to Snell's law, as shown at Figure 3-11.

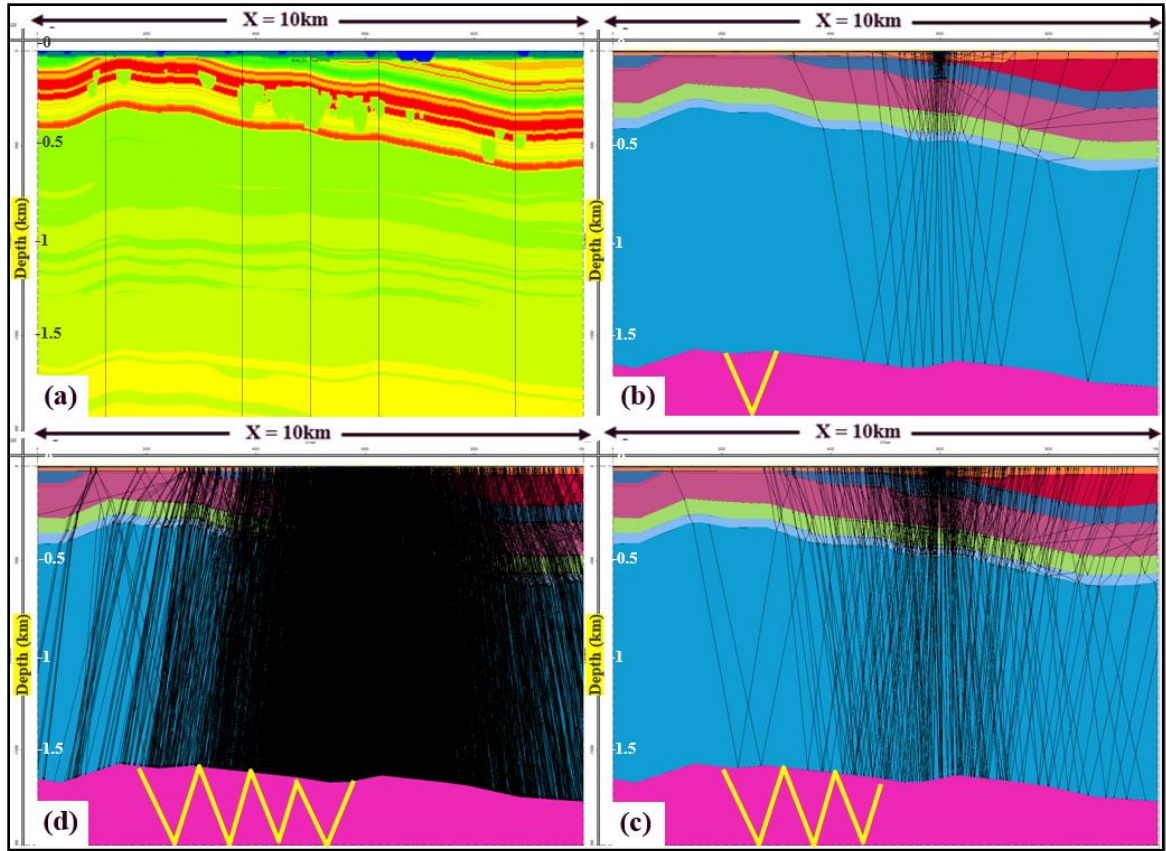


Figure 3-11: Interface based Arid SEAM model overlaid with raypaths (a) gridded model (b) interface based model overlaid with reflected P-wave rays (c) interface based model overlaid with reflected P-wave rays and 1st & 2nd order of multiples (d) interface based model overlaid with reflected P-wave rays and 1st to 3rd order of multiples

Figure 3-11 shows the ray tracing results for the layered model using one source point at a depth of 10m and rays out to a maximum offset of 6km. Figure 3-11b shows the reflection and transmission of primary rays at layer boundaries. Figure 3-11c depicts the ray paths of the primary reflections in addition to the 1st & 2nd order multiples. If we compute to 3rd order multiples all rays at top of the model in Figure 3-11c will act as new source points which reflect in the model, as shown in Figure 3-11d.

After we demonstrate the ray paths for one shot for a 2D interface model, we used the arid SEAM 3D gridded model to generate rays at different locations in 3D space and generated

hit count maps to demonstrate the illumination variation due to a complex near-surface geology.

We consider three scattering points in the subsurface below the near-surface zone. Each point scatters rays at all azimuth directions up to 50deg dip angle. Figure 3-12 shows the propagated rays from these scattering points to the surface for the four different models. Figure 3-12b shows some rays reflected down at top of LVL around 350m depth. These downward reflecting rays are more dominant in Figure 3-12c, where there is a strong velocity inversion which produces short and long period multiples.

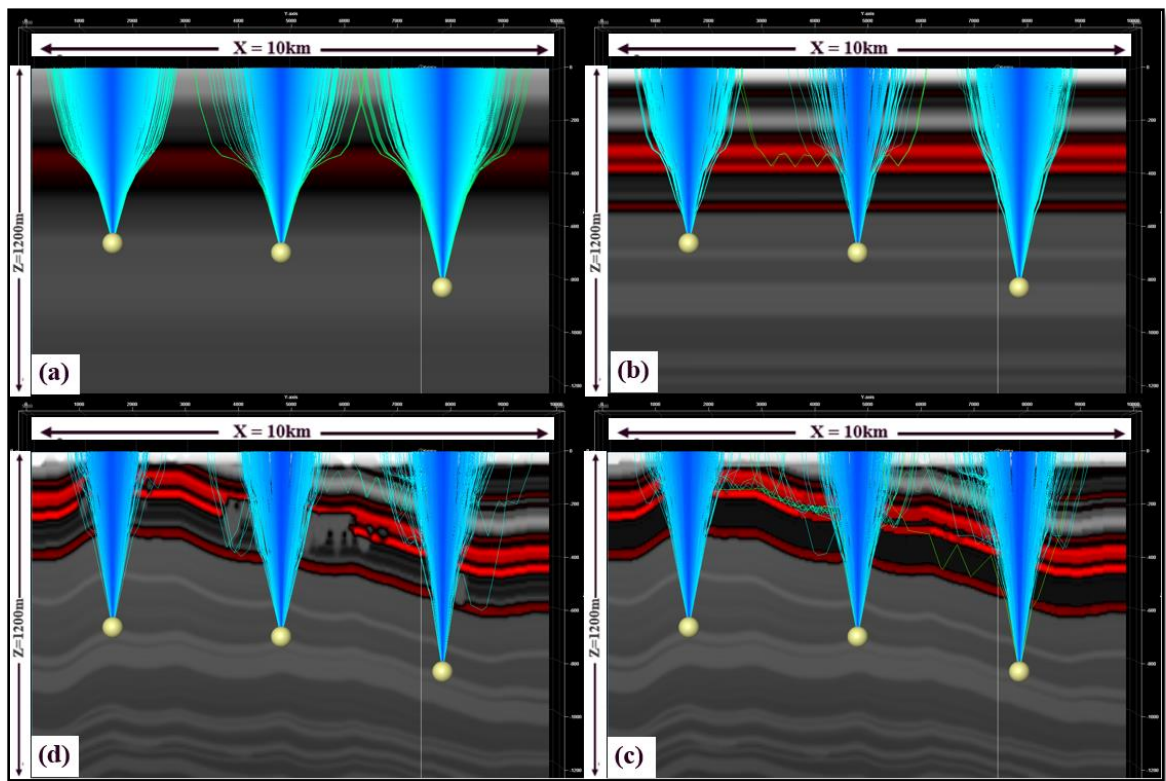


Figure 3-12: 2D view of ray paths colored with offset overlaid over velocity model shows the rays are trapped within low velocity layers (a) smoothed 1D model (b) complex 1D model (c) complex 3D model (d) complex 3D model with Karst.

Figure 3-13a shows a grid of scattering points at a depth 200m below the base of the carbonate layer, whereas Figure 3-13b shows the structure map of the shifted base carbonate surface overlain by five scattering points (marked in red) over the 3D model.

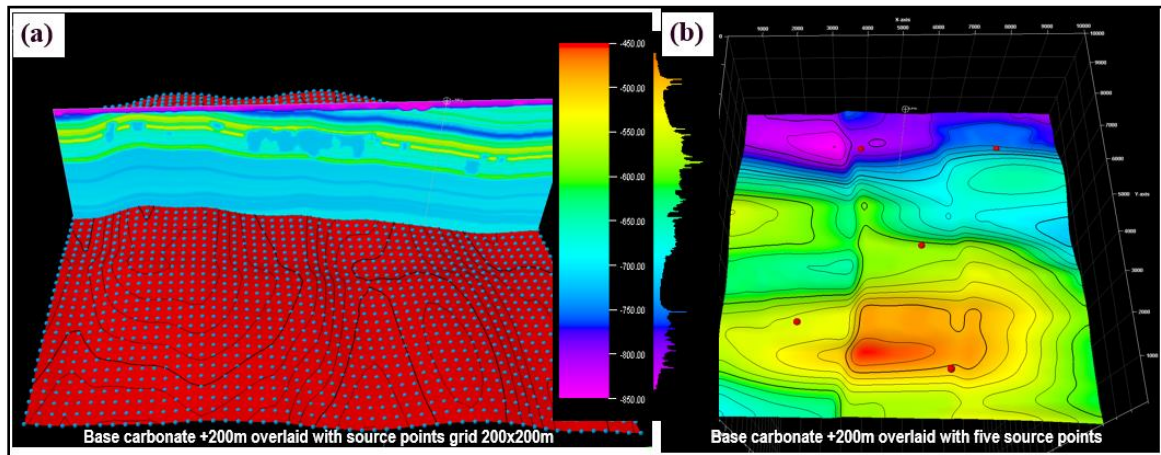


Figure 3-13: Base carbonate horizon shifted down by 200m (a) horizon overlaid with shot grid 200x200m (b) horizon overlaid with five source points over the model.

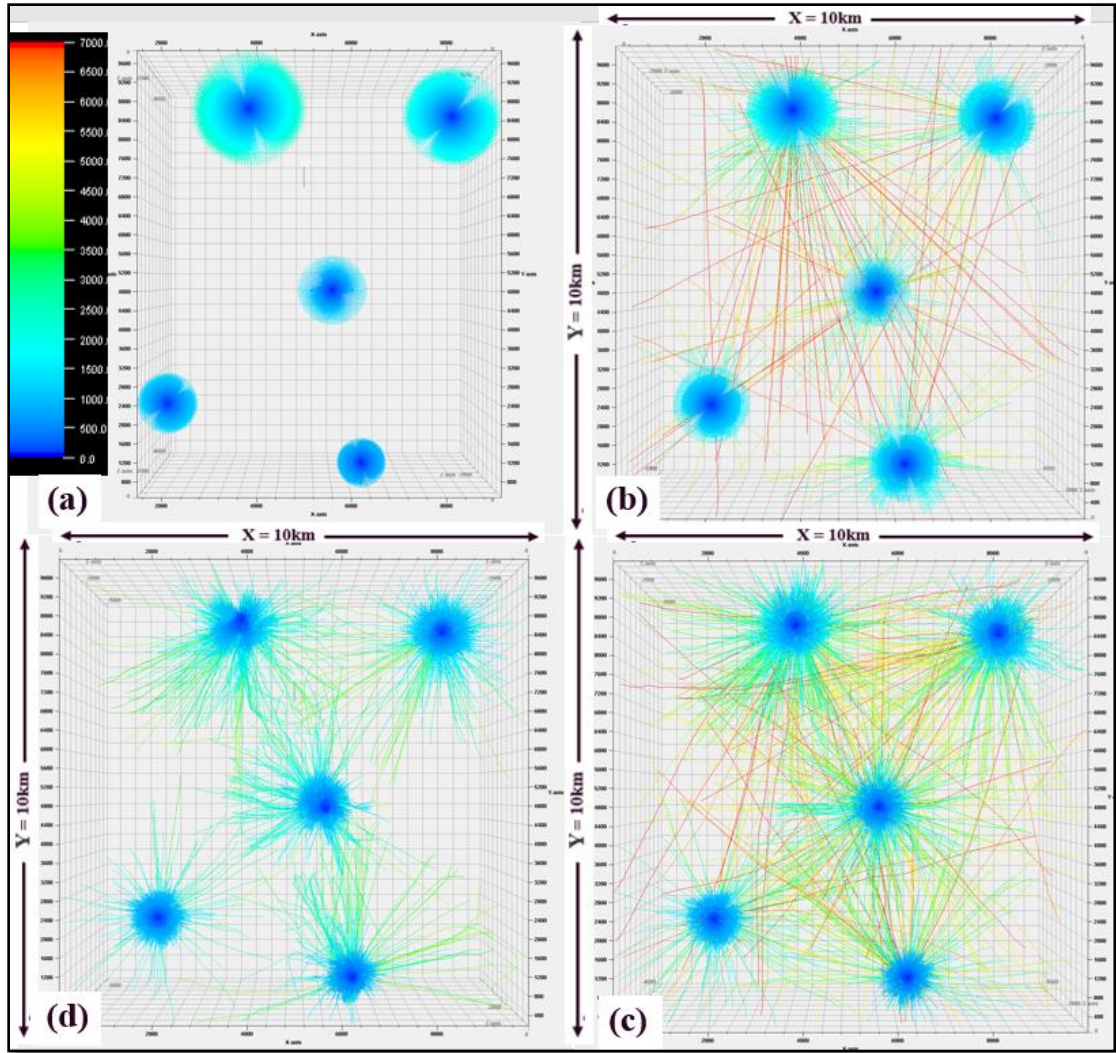


Figure 3-14: 3D ray paths view at top of the model (a) smoothed 1D model (b) complex 1D model (c) complex 3D model (d) complex 3D model with Karst.

Figure 3-14 illustrates some rays that are trapped (bounce back and forward) within the low-velocity layers, which demonstrates the association of interbed multiples with strong velocity inversions.

We can see complex illumination variation due to strong near-surface heterogeneities as shown in Figure 3-15.

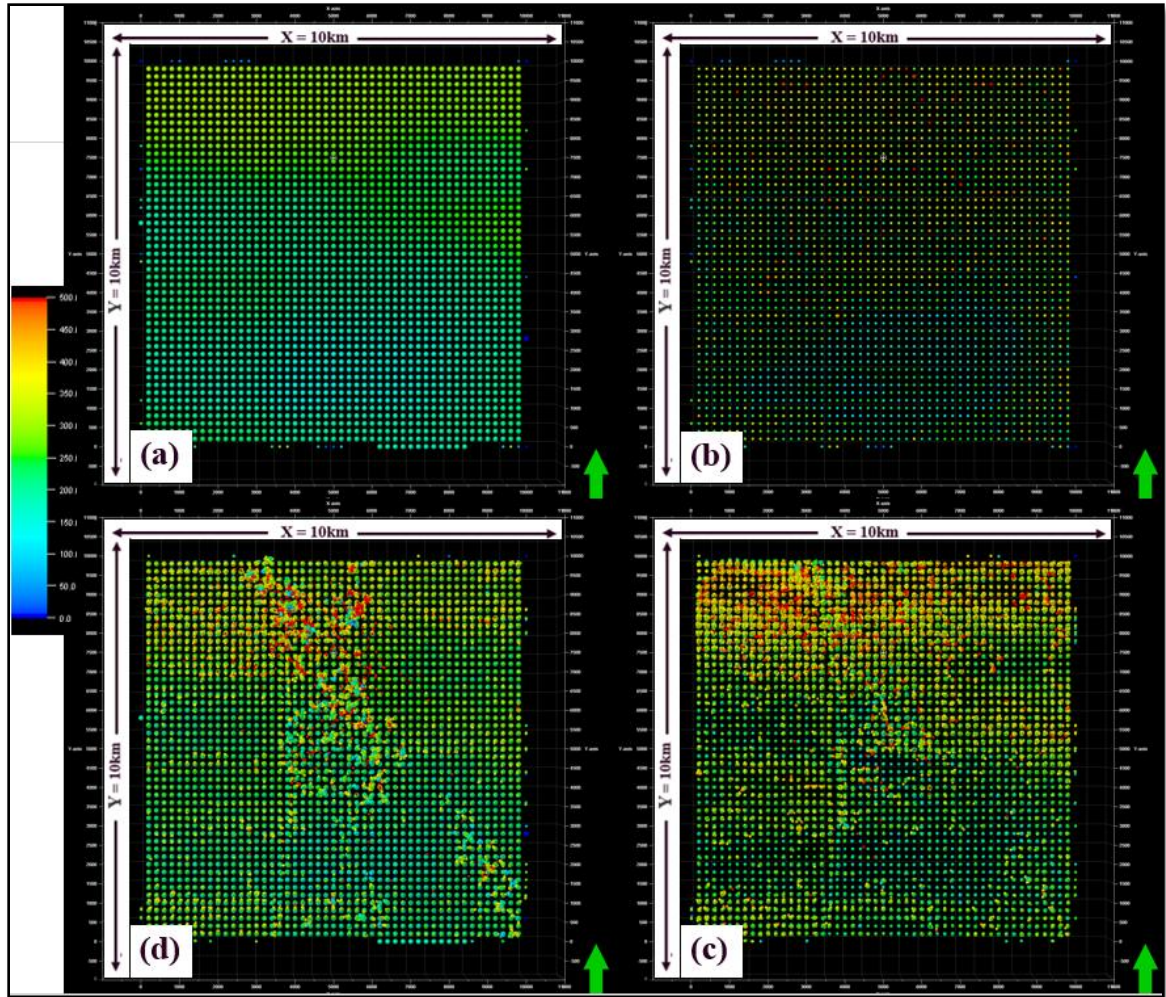


Figure 3-15: Hit count and offset ray maps for (a) smoothed 1D model (b) complex 1D model (c) complex 3D model (d) complex 3D model with Karst. The Hit count maps show illumination heterogeneities due to the overburden effect of the complex near surface.

3.6.2 Finite difference method

The finite difference forward modeling methods involve the numerical solution of the seismic wave equation. The finite difference method is one of these methods which yields the entire seismic wave response at any point in the geological models. We simulate one acoustic synthetic shot at 5km offset for four different models (shown in Figure 3-10). The result of this simulation is shown at Figure 3-16.

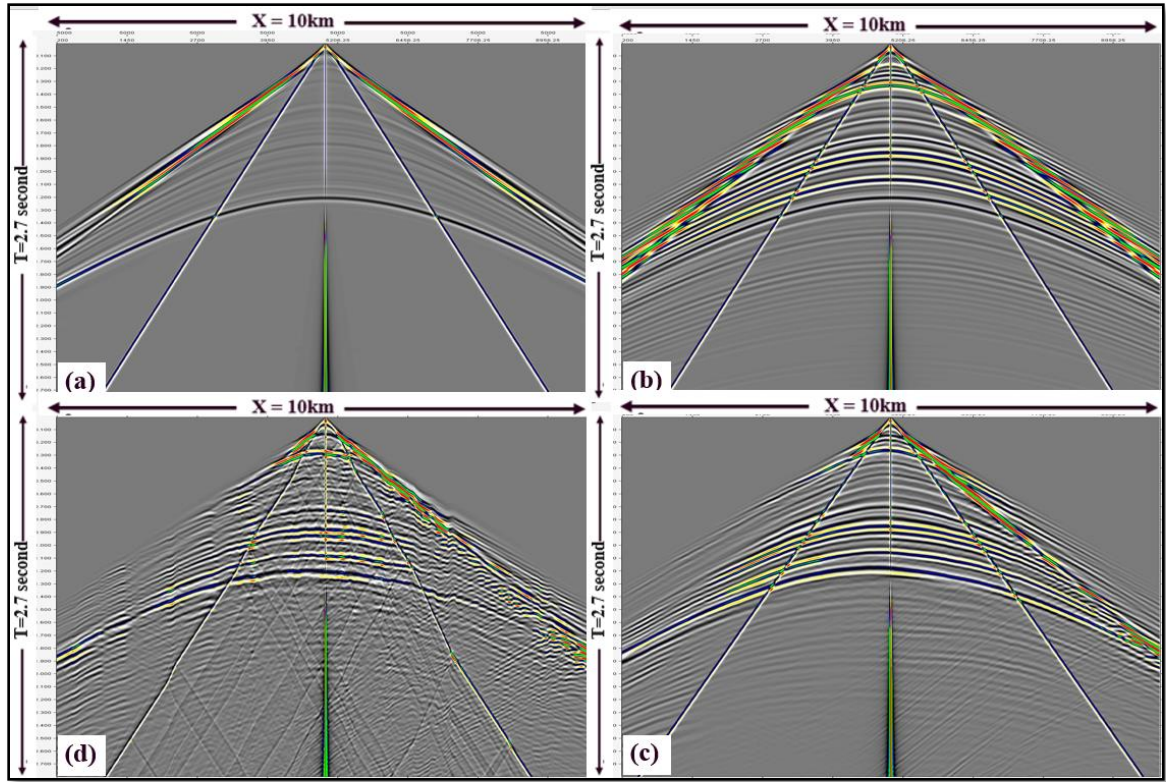


Figure 3-16: Synthetic acoustic shot at offset 5km of (a) smooth 1D model (b) complex 1D model (c) complex 3D model (d) complex 3D model with Karst. Strong velocity inversion generates strong internal multiples and guided waves and Karst scatters the seismic energy.

The synthetic shot gather of the smoothed 1D velocity model is shown at Figure 3-16a; It shows a homogenous p-wave without interbed multiples and with symmetrical hyperbolic reflection events. It also has clear and continuous first arrival energy. Figure 3-16b shows the simulated shot of the 1D velocity model with strong vertical velocity changes which has discontinuous first arrival energy (shingling phenomena) and interbed multiples due to the strong velocity inversion. Figure 3-16c represents the synthetic shot gather of the complex velocity model but without Karst. The gather has a complex first arrival pattern, guided waves and asymmetrical primary and multiple reflections due to the complex structure and stratigraphic features that exist in Arid SEAM model. In Figure 3-16d, the synthetic shot of the Arid model that illustrates well the phenomenon of p-wave scattering

energy due to irregular shape, size and distribution of Karst geobodies at and near the surface which introduce strong velocity contrasts, hence diffracted energy..

After we understand the behaviour of acoustic seismic waves for the four models with different geological scenarios, we now examine the other seismic wave propagation model types (elastic, viscoelastic and viscoelastic with multiples) by generating synthetic shot gathers from the Arid SEAM model with different finite difference modeling schemes; in particular the acoustic, elastic and viscoelastic without/with free surface multiples as shown in Figure3-17.

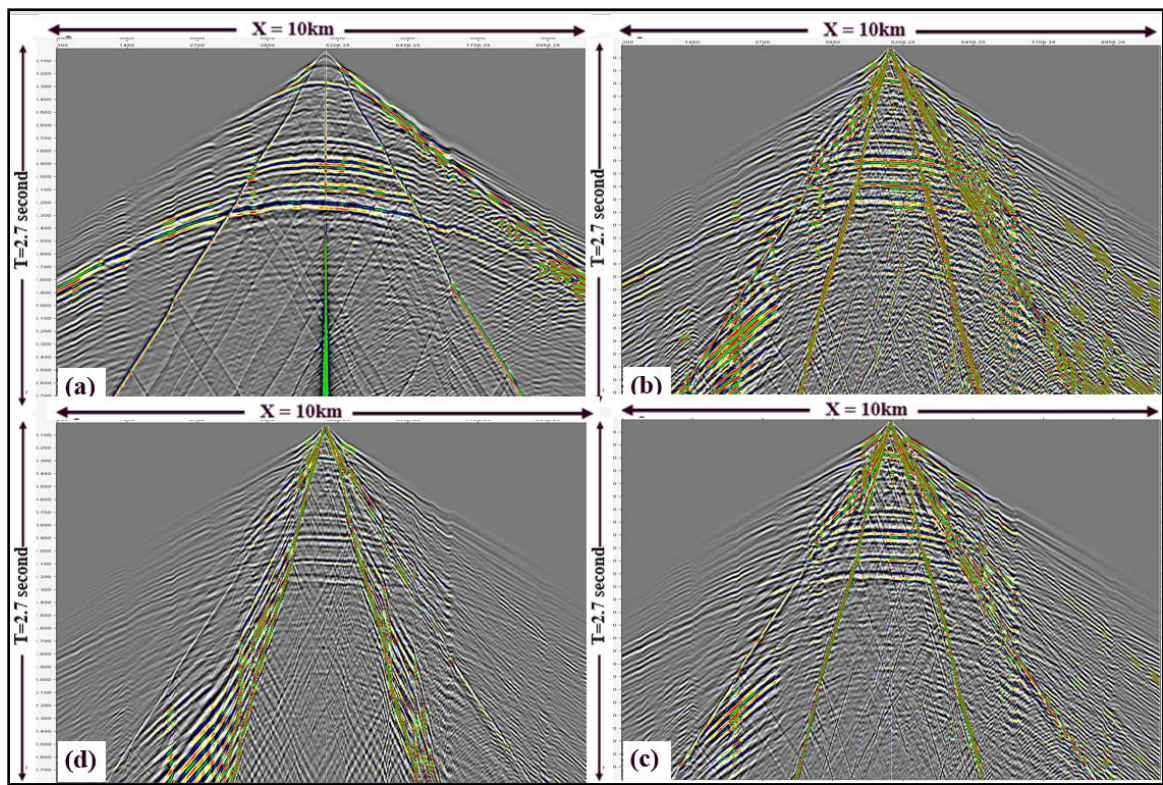


Figure 3-17: synthetic shot in the middle of Arid model (a) acoustic wavefield (b) Elastic wavefield (c) Viscoelastic (d) Viscoelastic with multiples. Viscoelastic synthetic data with multiples are very correlate with real seismic data where dispersive ground roll, converted and shear waves are dominating the recorded land seismic data.

By examining these four wavefields, we observe that the acoustic wavefield has strong guided waves and energy due to multiples associated with strong velocity inversion. The

elastic wavefield gives a better match with real seismic data where surface waves predominate and their dispersion due to strong lateral velocity variation is well observed. By increasing the wavefield complexity through viscoelastic models with free surface multiples yields the synthetic data which correlates well with real seismic data. This affirms the importance of absorption and scattering in the geological column.

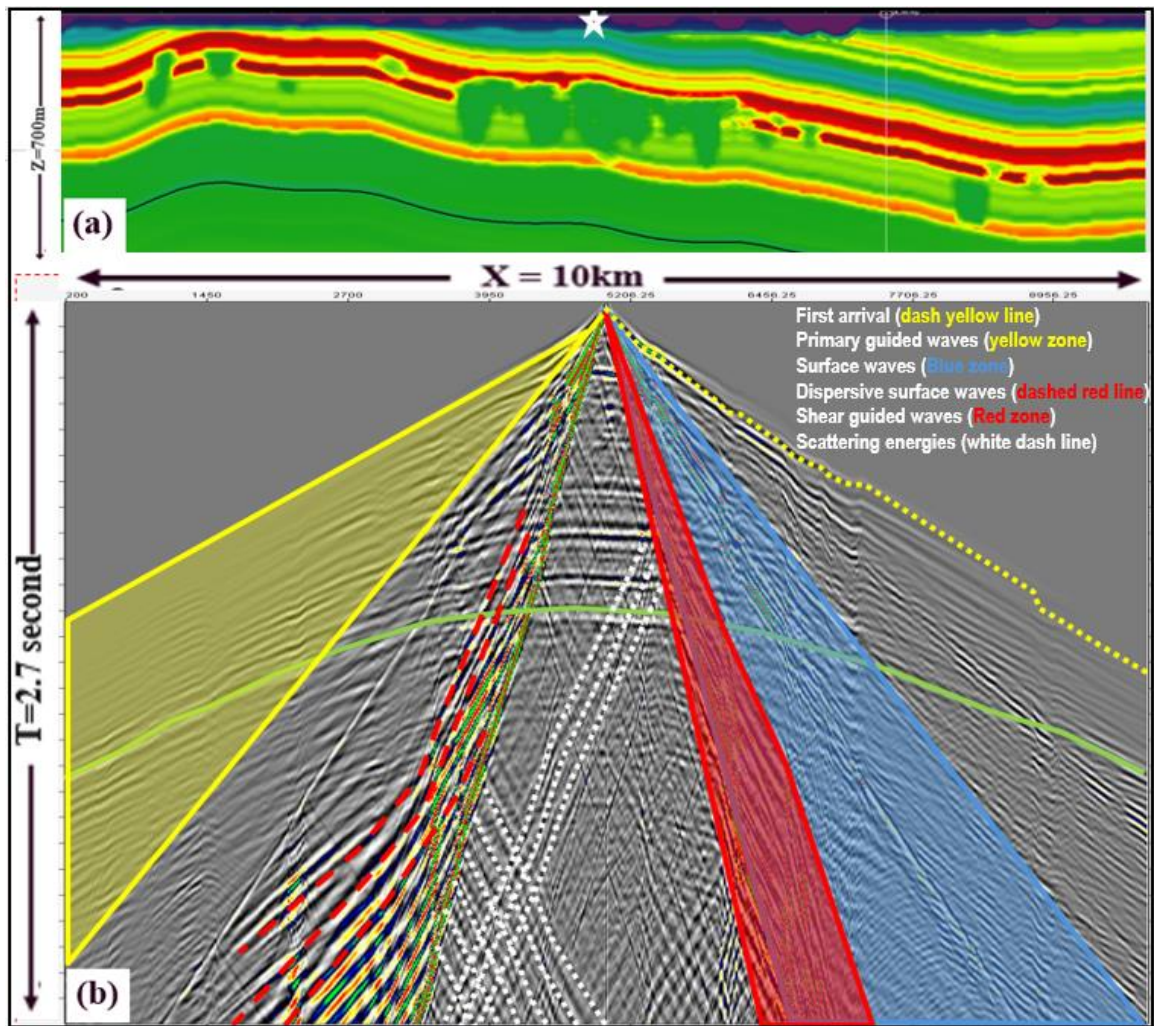


Figure 3-18: Interpretation of seismic wavefields (a) near-surface velocity model (b) viscoelastic synthetic shot overlaid with interpretation zones and horizons.

Figure 3-18 provides the interpretation of the seismic wavefield for viscoelastic synthetic shot with multiples. The yellow zone represents the guided wave energy, the dashed yellow line marks the first arrival energy (direct and refracted waves) which shows the complex

static issue. There is a good correlation with the surface Karst locations in the velocity model at Figure 3-14a. The Rayleigh wave zone is highlighted in blue color. It overlaps the guided shear waves highlighted in red. Dispersive surface waves are a direct indicator of a complex near-surface velocity variation which are delineated as the dashed red events. Scattered energy due to the irregularity of Karst size, shape and distribution are highlighted as white events. Any parabolic or hyperbolic events that arrive at a later time than the green horizon are primary and/or multiples of the shear waves or multiples of the primary waves.

3.7 Discussion and conclusions

The Arid SEAM Phase II model has complex near-surface features including Karst, wadis, stream channels and low-velocity unconsolidated sediments in the near-surface introduce strong velocity contrasts that generate extreme near-surface signal scattering often seen in real seismic records from arid terrains.

The modeling study helped to understand the characteristics of the recorded seismic data in the Arabian Gulf. The ray tracing through the Arid SEAM model showed how the Karst bodies can dramatically change the behavior of the wave path.

We also saw the effect of each property of the Arid SEAM model on the recorded seismic data. Starting from the general 1D velocity trend, passing through the effect of strong vertical velocity variations and ending with the full complex 3D geology involving various dips and karst structures. We can clearly observe the scattering of waves because of Karst. In addition, the presences of multiples in the seismic data cannot be under-estimated; the strong velocity contrast between the layers and the presence of complex structures makes

free surface-related and interbed multiples a significant challenge for land seismic exploration.

The viscoelastic modeling showed the effect of absorption on the amplitudes of multiples and primaries. It is well understood that at longer times (greater depths), the signal-to-noise ratio is expected to decrease substantially especially with the presence of higher modes of ground roll and the rapid attenuation of primary energy as a result of absorption and scattering.

The shallow Karst structures leave an imprint on the seismic gathers. This includes undulations in the first arrivals approximately at the same locations as the Karsts. The fact that the imprint of Karst is well observed on the refractions in the seismic gathers points to the importance of refraction (diving wave) FWI in resolving such complex structures in the velocity model.

Finite difference and ray tracing experiments successfully demonstrated the complexity of seismic wave propagation in areas with variable near-surface geology like the one represented in arid SEAM model. In next chapter, we will examine the behavior of FWI with such a complex model.

CHAPTER 4:

Acoustic FWI on acoustic and viscoelastic synthetic data

I will examine in this chapter if Acoustic FWI can accurately reconstruct models of small, shallow geological features with strong velocity contrasts such as the Arid SEAM model, so as to improve seismic subsurface imaging.

4.1 Requirements for FWI success

Before starting a FWI project, we should consider the following two critical factors to ensure a successful result.

1. A good starting velocity model. FWI is a model updating method and it relies on a starting model being close enough to the true model for the inversion to converge to the correct model, which is generally known as the global minimum. If the starting model is too far from the correct model, FWI might still converge but to one of the many local minima
2. The input data should contain a broad range of frequencies and a sufficient offset range in the recorded data. The low frequency content in the data is important to get a stable inversion at low frequencies to avoid cycle skipping. The offset range and high frequency content is important for getting adequate resolution at depth. Typically for refraction or diving wave FWI, we expect reliable results down to a depth of about one half to one third of the maximum offset.

4.2 FWI workflow

In this section, we introduce more detailed information about acoustic FWI workflow and the key steps, starting from the input data preparation, source wavelet, initial model and starting frequency, as well as gradient smoothing and line search

4.2.1 Input data preparation

As the recorded data will be compared with modeled data, it is important that the preparation and pre-processing of the data makes it as comparable as possible with modeled data.

Modeled data does not contain noise. Therefore, we established random and coherent noise suppression workflow to remove only those aspects of the field data that the acoustic forward scheme is not intended to simulate (e.g. shear waves, surface waves and tube waves), while carefully preserving refracted and reflected body wave. The results of these processes are shown in Figure 4-1.

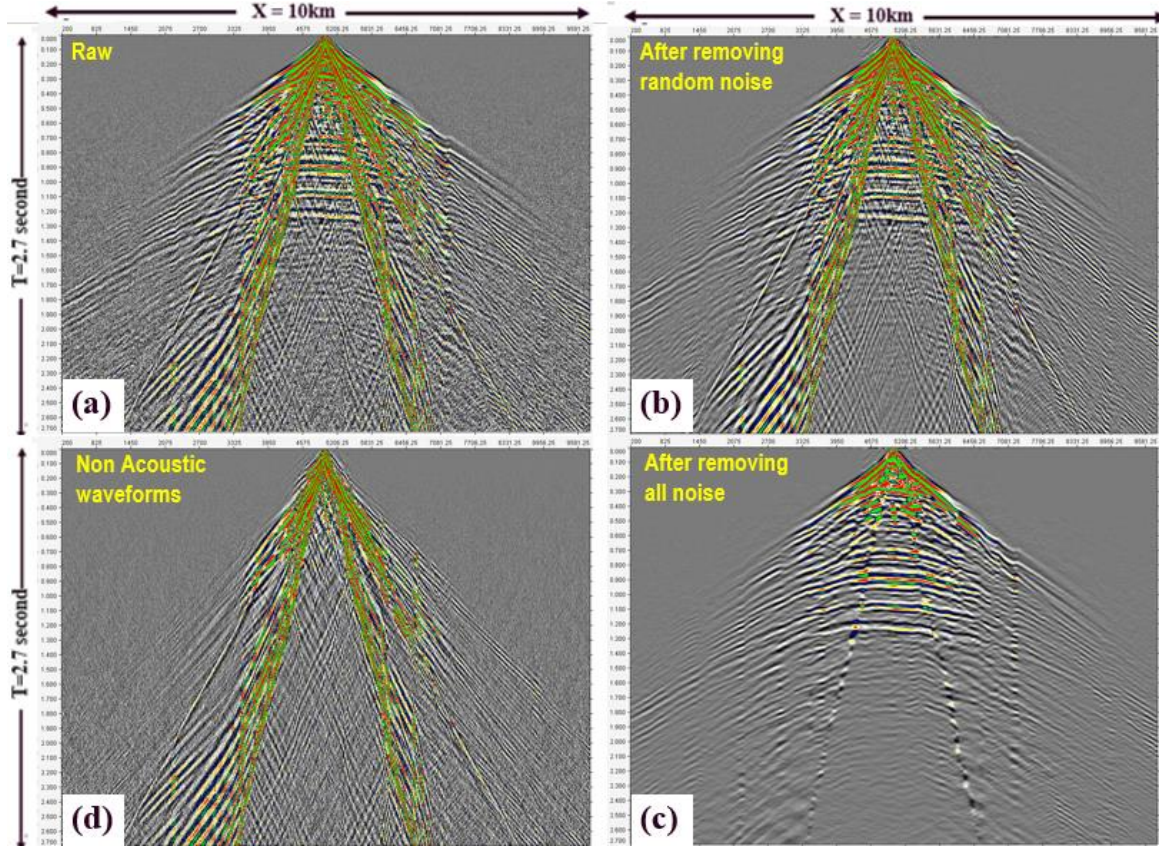


Figure 4-1: Data conditioning result, (a) raw shot gather, (b) shot gather after random noise attenuation (c) shot gathers after random & coherent noise attenuation (d) removed energies by noise attenuation application. Noise attenuation techniques suppress most of elastic and coherent noise and provide a better input to the acoustic FWI.

4.2.2 Source wavelet

FWI aims to minimize the least squared difference between the predicted and observed seismic responses by means of updating the model on which the prediction is based. Because the predicted and actual seismic responses are functions of the model parameters as well as the source signature, a good estimate of the source wavelet is important for the update and convergence in FWI.

We consider it safer to extract the source wavelet from the data itself. This is done as a separate inversion step and the result used in subsequent inversion passes over that frequency band.

4.2.3 Starting Model

The starting model should contain those spatial frequencies (wavenumbers) that are not within the seismic bandwidth (e.g., low frequencies) and thereby ensure a bridge between the frequencies in the starting model and the temporal frequencies in the data.

Velocity scanning and manual velocity picking methods have been used to determine the initial 2D general velocity trend, the surface wave inversion was used to estimate more accurate velocity at first 200m in the model as discussed in next sections

4.2.3.1 Determination of the stacking velocity

The initial velocity model has been estimated from the input seismic data itself using the velocity scan approach (stacking velocity analysis) to determine initial 1D velocity function (its results are shown in Figure 4-2). This function has been used as central component for manual velocity analysis

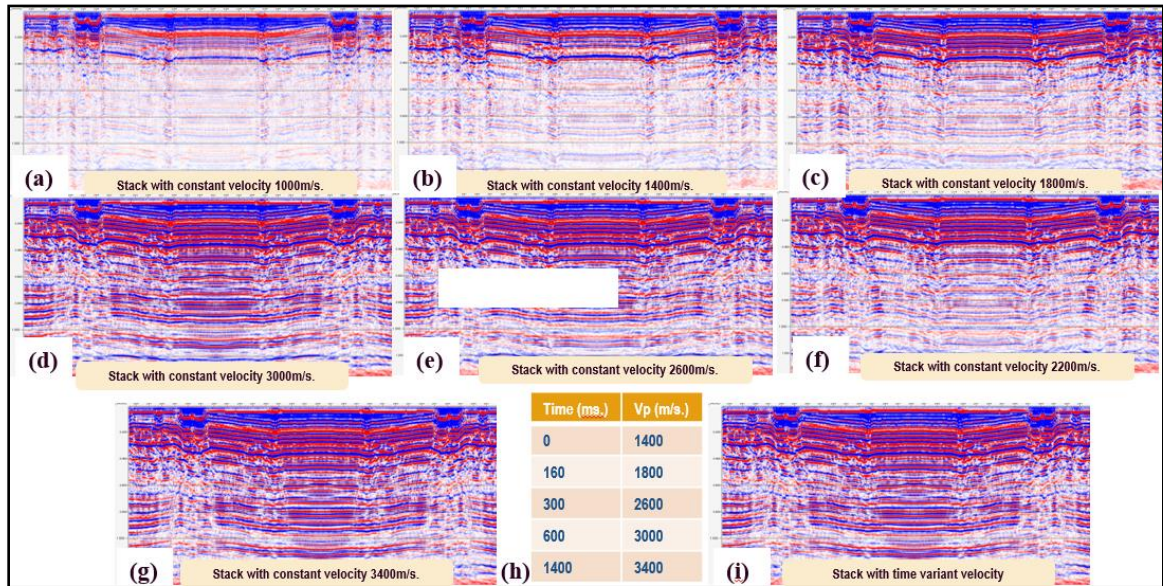


Figure 4-2: Stacked section with different constant velocities, starts from $V_p=1800$ - 3400 m/s every 400 m/s increment as shown from (a) to (g), (h) shows values of optimum 1D stacking velocity and its stack at (i).

Manual velocity analysis is done at every 500m location over the 2D line in order to determine the best stacking velocity based on semblance, gather flattening and stacking power. Figure 4-3 shows all displays that help to obtain best stacking velocity at one of the locations in addition to the velocity overlay on the stack to confirm its conformability with the geology.

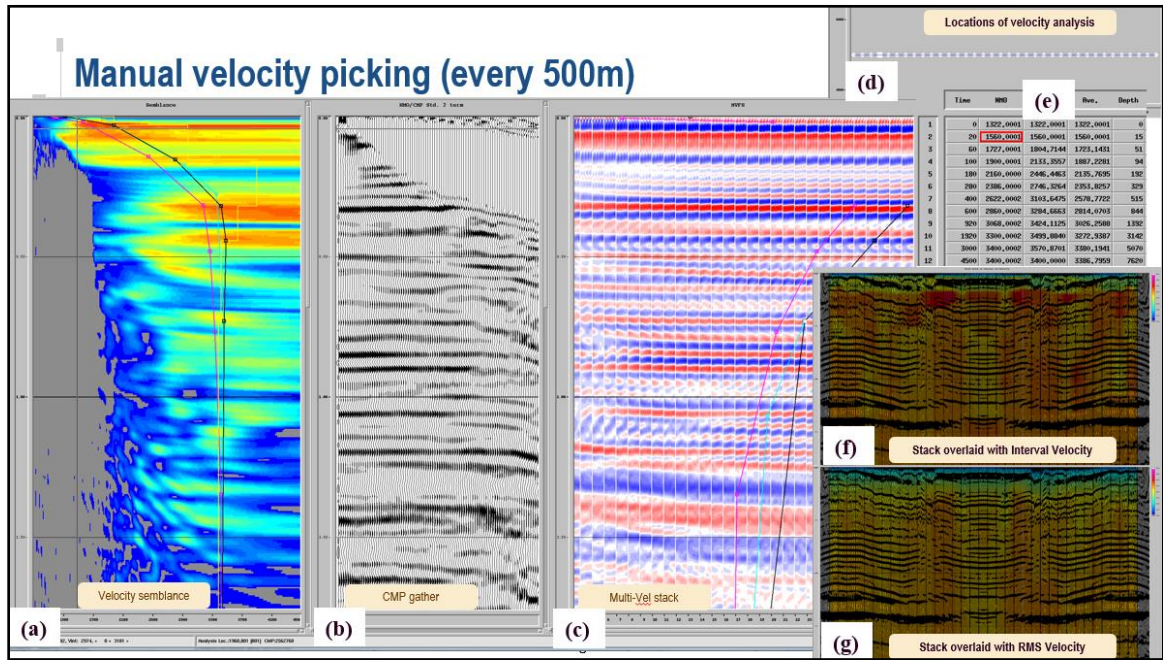


Figure 4-3: Manual velocity picking QC and displays (a) semblance, (b) CMP gather, (c) multi-vel stack panels (d) Map shows velocity location every 500m, (e) table shows RMS velocity value of the current location and its interval and average (f) stack overlaid with interval velocity (g) stack overlaid with RMS velocity.

Further higher velocity update at very shallow part, has been achieved through surface wave analysis and inversion.

4.2.3.2 Very shallow-velocity update using SWI

Surface waves propagate horizontally within inversion to estimate V_s . the near surface, parallel to the free surface, and with cylindrical wavefronts. Surface wave inversion (SWI) provides more detailed and accurate information about the inhomogeneous medium typical

of the near-surface by analyzing the surface wave in the frequency-wavenumber FK-domain to obtain phase velocity ($C = w/k$) -vs frequency (or wavelength or wavenumber)) curve at each surface location which is then inverted using iterative damped linear least-squares single domain inversion to estimate Vs vs depth

SWI provides a detailed 2D or 3D spatial near-surface Vs model. It can then be converted to Vp using the Vp/Vs relationship from uphole, well logs, or an empirical relationship. In this thesis $V_p/V_s=2$ has been used.

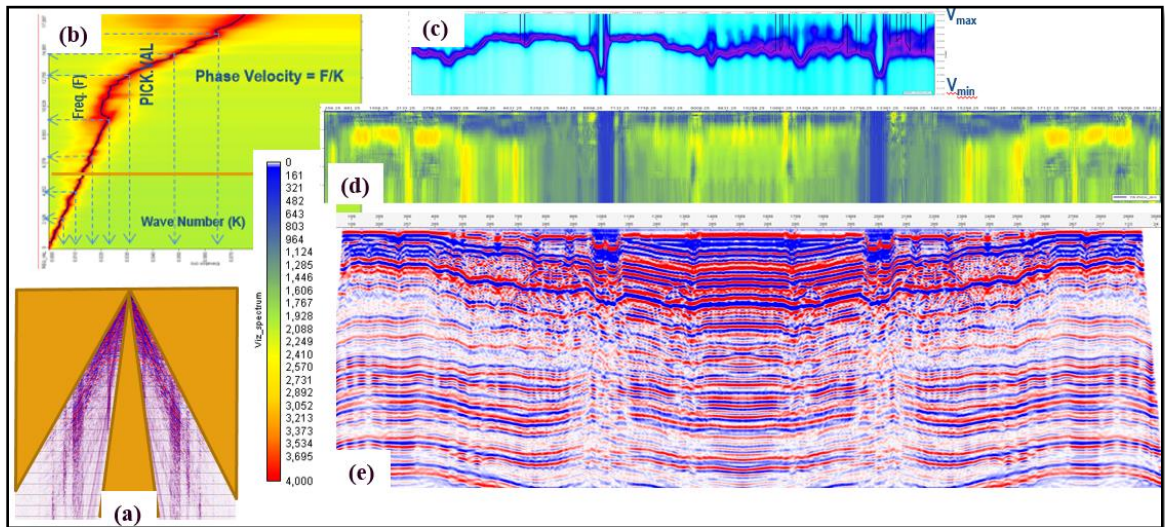


Figure 4-4: Surface wave inversion steps (a) windowing the surface wave energy (b) pick high semblance of its FK spectrum at all surface locations (c) a display of picks overlaid on semblance of all locations at certain frequency (d) Vs velocity inversion (e) stack shows good correlation between inverted velocity and Karst locations.

For the initial model evaluation and validation as well as quality control (QC) the impact of the very shallow-velocity distribution which is determined by inverting surface wave energy. We migrate the input data using both velocity models through RTM as shown in Figure 4-6.

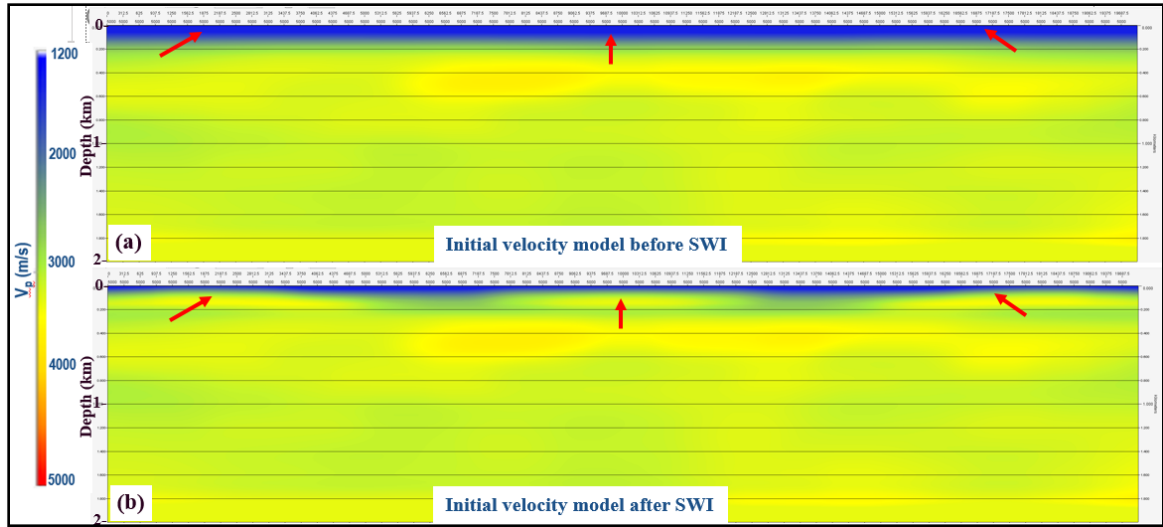


Figure 4-5: SWI provided more accurate velocity at top 200m (a) velocity from manual picking (b) velocity after SWI update.

Figure 4-5, shows the velocity update at the top 200m in the model using SWI. This technology can update the velocity model more accurately at the very shallow part by utilizing the surface wave information that leads to better definition of the limestone velocity in the shallow part of the section. Consequently, the RTM global image improved dramatically at the shallow depth as well as the deeper section as shown in Figure 4-6.

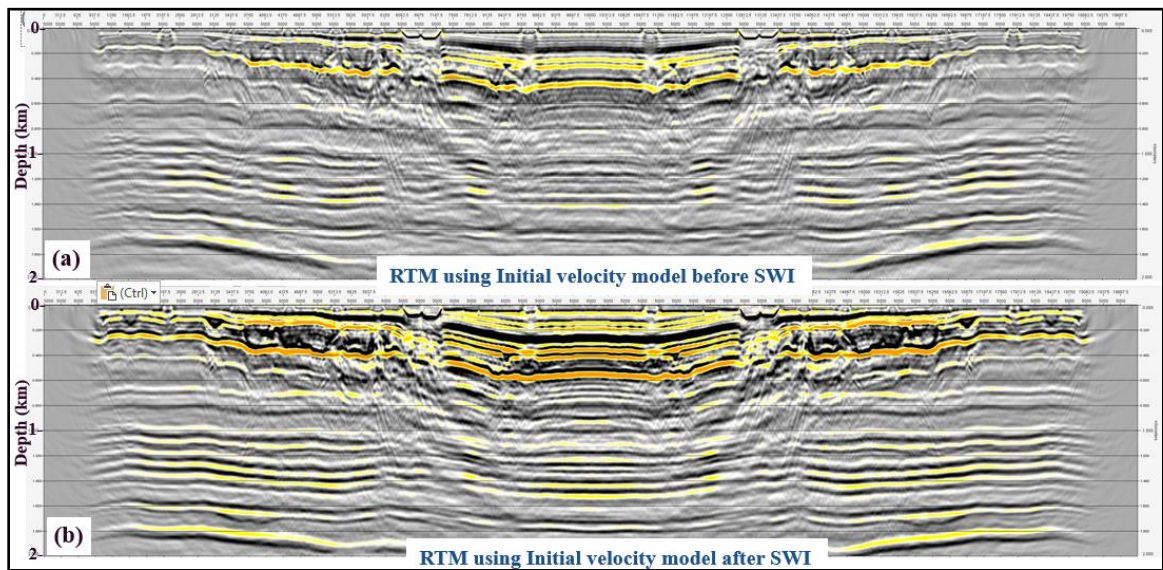


Figure 4-6: RTM Global Image using initial model, (a) before SWI update, (b) after SWI update at bottom. SWI provides more accurate velocity at shallow part of the model which has a dramatic improvement on the subsurface image.

SWI improves the accuracy of the starting velocity model of FWI which helps us to invert the source wavelet from the data itself without any assumption about the wavelet attributes. By improving the main FWI inputs, the possibility to converge to the global minimum through FWI will increase.

4.2.4 Which data to include?

A crucial question is which part of the data should be included in the inversion. Depending on which part of the model is being updated and the accuracy of the model at any step, different parts of the data might be included in the residual calculation and inversion. We start with early arrivals to provide the low-wavenumber solution at low frequencies 4, 6 and 8Hz. Once a good and detailed model has been resolved then we start FWI using refracted and reflected events which was carried out at 8 & 12Hz frequency bands.

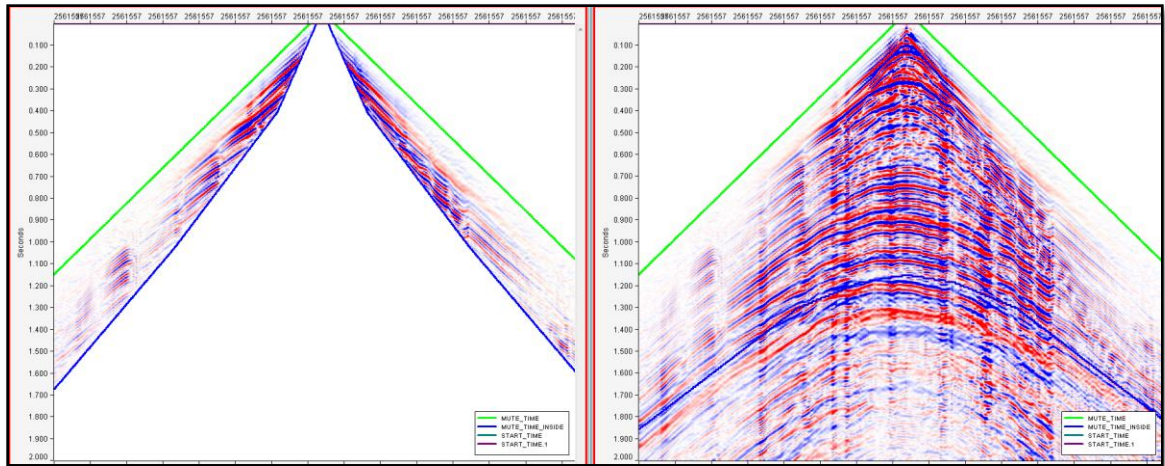


Figure 4-7: Shot gather input to FWI (a) early arrivals only (b) both refraction and reflection events.

Figure 4-7 shows the mute functions which have been used to preserve the early arrival refraction events only at low frequency FWI on the left side and at the right of the figure.

Refraction and reflection events within the green and blue curves are used for higher frequency bands of FWI.

4.2.5 Objective function

FWI minimizes the difference between observed and modeled data in a linear least squares sense. This is referred to as the least square objective function. We have used two methods to calculate misfit functions for inversion. We start the inversion with the travel time error function to update the model and reduce the possibility of local minimum trapping when using least square waveform objective functions at later iterations.

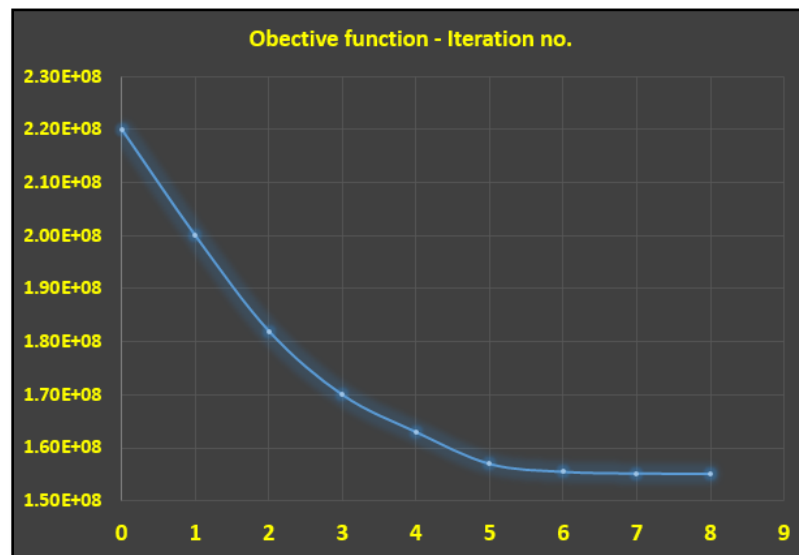


Figure 4-8: Graph shows an example of the reduction of objective (misfit) function with inversion iterations at FWI 6Hz. The graph shows the reduction in mist-fit function starts to be stabilized from iteration 5.

Figure 4-8 shows the reduction of least square objective functions with inversion iterations during early arrival inversion at peak frequency 6Hz. The graph shows the stabilization starts from iteration 6 forward, so we choose iteration 06 update as the input for the next frequency band.

4.2.6 Frequency bands

Currently FWI must start from low frequencies to ensure convergence to a global minimum. Once the inversion has converged at one frequency band, the inversion moves to higher frequencies, thereby adding more details to the velocity model. FWI needs to iterate over several frequency bands to achieve the desired model details. The number of frequency bands, iterations and type of data used for inversion are shown in Table 1.

Peak frequency	Maximum frequency	Inverted energy	No. of iteration	Objective function
4	7	Refraction	4+6	TT+LS
6	11	Refraction	3+5	TT+LS
8	14	Refraction + Reflection	5+6	LS
12	21	Reflection + Reflection	6+6	LS

Table 1: FWI over four frequency bands using refraction and/or reflection events with different objective function methods.

4.2.7 Gradient smoothing

Gradient smoothing is a crucial step for conditioning the gradient before being used in the line search which damps out oscillations in the velocity updates and can lead to faster convergence.

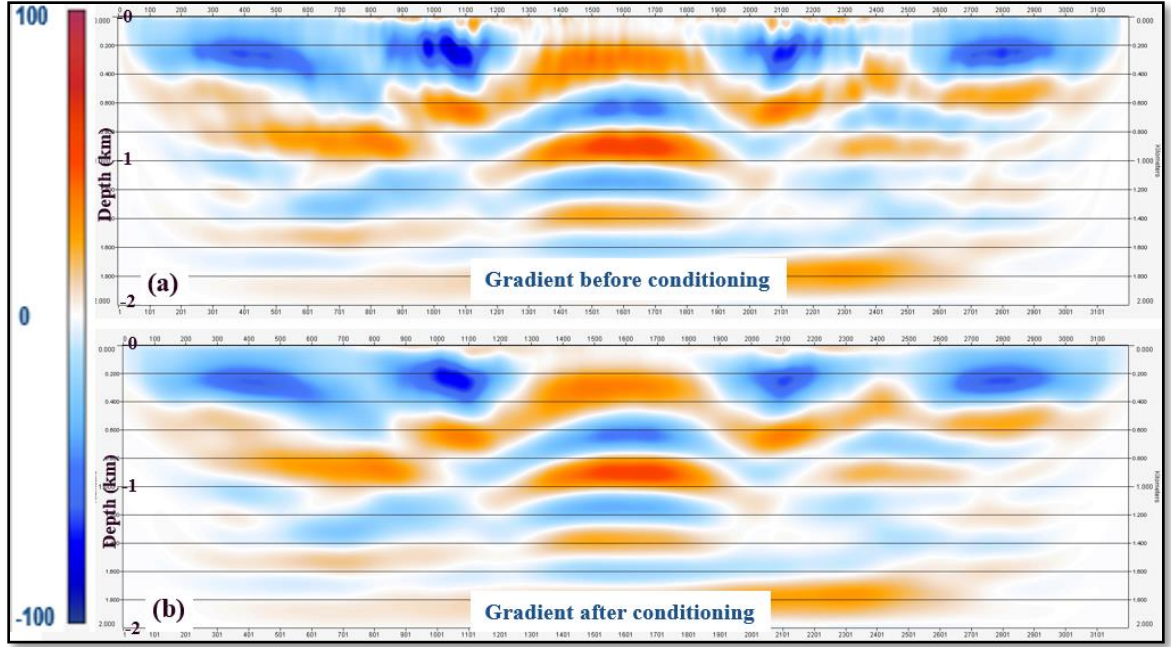


Figure 4-9: Gradient conditioning (a) before conditioning (b) after conditioning. Gaussian smoothing filter helps to suppress the migration jittering and smiles at shallow part of the gradient.

Figures 4-9 shows the gradient section before/after smoothing which helps to remove jitters in the gradient file

4.2.8 Line search

The calculated gradient provides the direction and relative magnitude of the velocity update. However, it needs to be multiplied by a scaling factor to get the globally optimum velocity update. The perturbation value, also known as the step length, is α in the following formula used in the velocity update:

$$c_{n+1} = c_n + \alpha \gamma_n \quad (8)$$

where c_{n+1} is the updated velocity model, c_n is the pervious iteration velocity model, α is the perturbation value and γ_n is the gradient function.

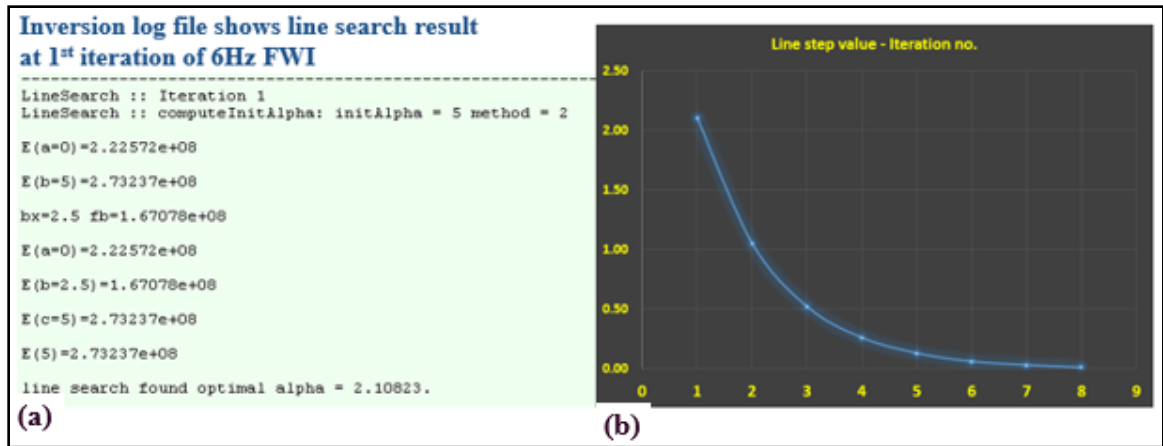


Figure 4-10: Line search method (a) log_file of step length trail at 1st iteration, (b) graph shows values of optimum alpha decrease with iterations.

Two forward modeling runs performed to determine the objective function value at $\alpha = 2.5$ and 5 then parabolic fitting is used to define the optimum alpha value which was 2.1 as shown at the inversion log file in Figure 4-10, in the same figure a graph shows the value of the optimum alpha decreases with increasing iterations which means the magnitude of the velocity perturbation decreases with iterations as shown in Figure 4-11.

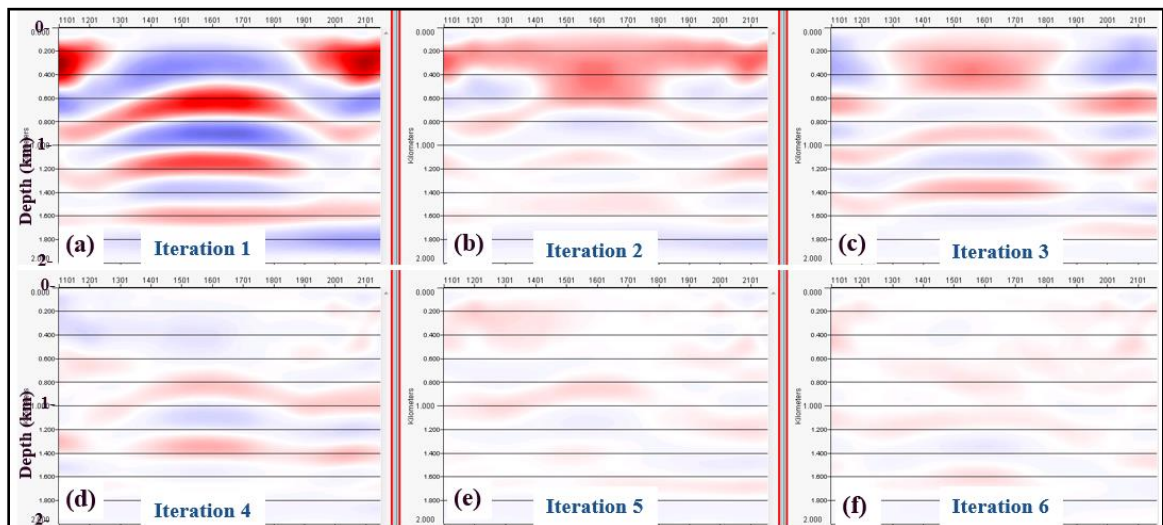


Figure 4-11: Vp perturbations from different iterations at 6Hz FWI. The velocity change reduces with iteration as indication of stabilization in the objective function and the convergence.

4.3 Case study-1: Acoustic FWI on acoustic synthetic data

An acoustic FWI workflow has been executed on two different synthetic data sets which we consider to be two case studies. The input of the first case study is the acoustic synthetic data which is simulated without free-surface multiples and noise and with a 50Hz Ricker wavelet. By contrast, the 2nd case study input data is much more complex than that of the 1st case study. It was simulated from a viscoelastic model and entails multiples and added noise. The source signal is Klauder wavelet with flat amplitude spectrum at 3-20Hz (as described in more details in section 3.4). Table 2 summarizes the differences between the two datasets.

	Case1- Acoustic	Case2 – Viscoelastic
Type of forward modeling	Acoustic	Viscoelastic
Vp & density relationship	Gardner	Variable
Wavelet	Ricker with max. 50Hz frequency	Klauder similar to Vibroseis (3-20 Hz)
Free-surface multiple	Not included	included
Noise	Not included	included
Starting model	Smoothed version of true model	Determined from seismic data
Maximum Frequency	50Hz	20Hz
Acquisition geometry	20km 2D line with SI=25m & RI=12.5m	20km 2D line with SI=25m & RI=12.5m
<div> <div>Case-1</div> <div>Simple Easy for FWI</div> <div></div> <div>Real Difficult</div> <div>Case-2</div> </div>		

Table 2: Two synthetic datasets generated with different input parameters and attributes: acoustic synthetic data in case-1 and viscoelastic with noise and multiples in case-2.

In this section, we will focus on the acoustic FWI result from the acoustic synthetic data of the 1st case study. As mentioned previously, the input is acoustic shot gathers without surface multiples and no added noise, so we don't need to apply any pre-processing before FWI. We invert over five frequency bands starting at 4 Hz and going up to 24Hz using refraction arrivals only, followed by reflection events at higher frequency bands as shown

in Table 3. The input velocity model in this case is a smooth version of the true model with smoothing operator length of 5000m in the horizontal direction and 500m in the vertical direction. The source wavelet is a Ricker wavelet of the same form as the synthetic wavelet.

Peak frequency	Maximum frequency	Inverted energy	No. of iteration
4	7	refraction	6
6	11	Refraction	6
8	14	Refraction + Reflection	4+6
12	21	reflection	5
24	42	Refraction + Reflection	5+5

Table 3: Acoustic FWI was performed over five frequency bands using refraction or refraction & reflection events with different number of iterations.

The objective is to examine if acoustic FWI on simple acoustic data can reconstruct the very small Karst features and the high-resolution details in the velocity of the SEAM model before we examine it on a full complex viscoelastic wavefield containing multiples and noise. Figure 4-12 shows that acoustic FWI successfully reconstructs the small Karst structures at very shallow depth and images accurately the strong velocity heterogeneity in the true model.

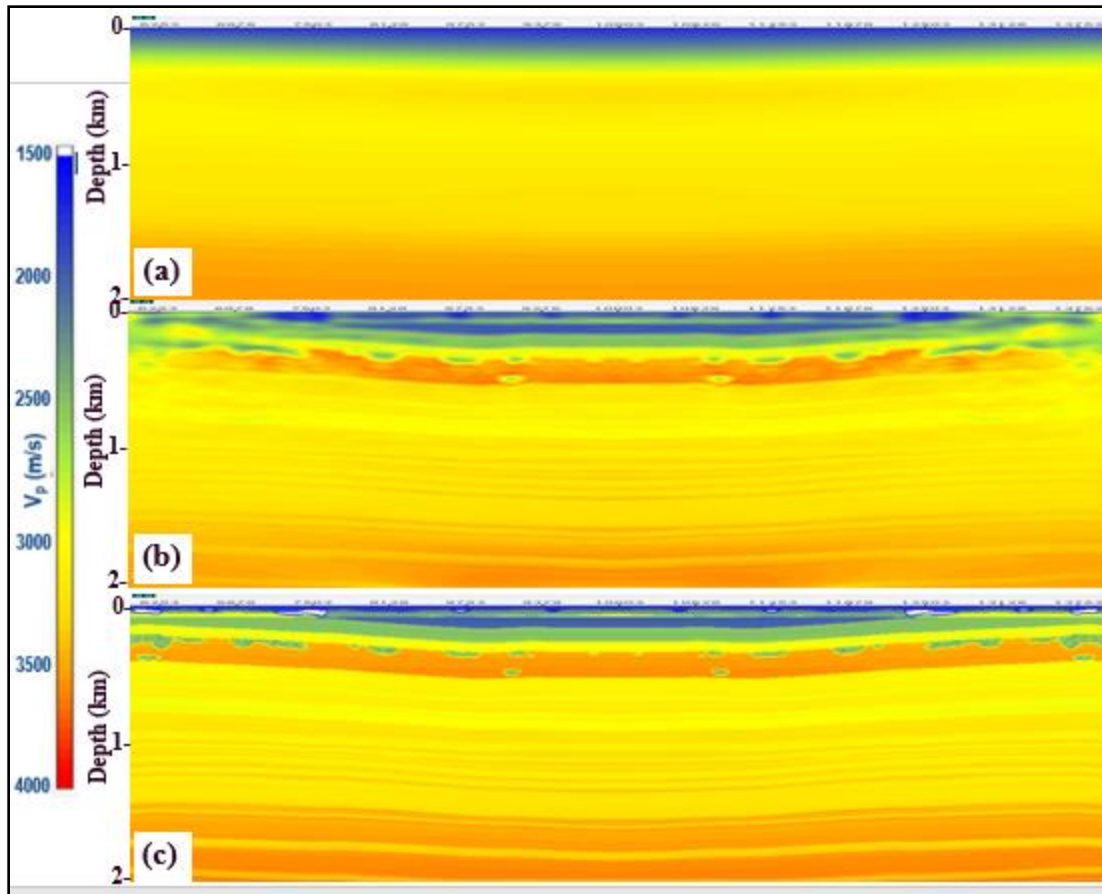


Figure 4-12: P-velocity sections show that FWI can reconstruct accurately the karst velocity and low velocity layers (a) initial model (b) estimated FWI model (c) true model.

Figure 4-13 shows the improvement in the RTM Global Image with the accuracy of the velocity model and the impact of being able to accurately reconstruct near-surface velocity variations on the subsurface image at deeper levels.

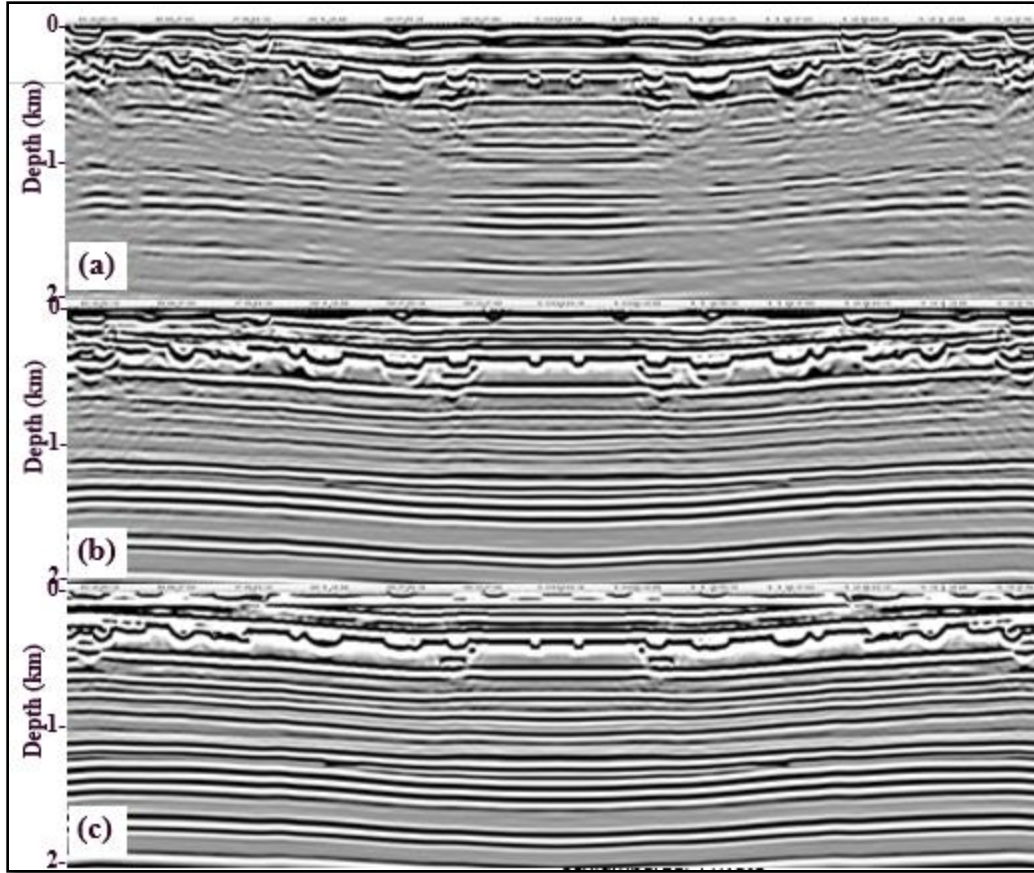


Figure 4-13: RTM Images of different velocity models (a) initial model (b) estimated model (c) true model. The subsurface RTM image comparison shows the similarity between the produced images using the true and estimated FWI models.

4.4 Case study-2: Acoustic FWI on viscoelastic synthetic data

In the second case study, we reduce the assumptions and simplification we made the first case study by using viscoelastic synthetic data with multiples and noise as the input to an Acoustic FWI code. Furthermore, we build the starting model from the seismic data itself without any contributions or influence from the known, true model. The source wavelet has been inverted from the data and not assumed to be known. The idea is to simulate the challenges that FWI faces on real seismic data.

To have a successful FWI result in this case several seismic processing methods have been used to have more accurate and better inputs to FWI which helps to reduce the possibility of local minima trapping. Firstly, we prepared the input shot gathers by applying noise attenuation processes to remove the energy such as surface waves that are not included in the acoustic forward modeling. This step is described in more detail in section 4.2.1. Secondly, we determine the starting velocity model by using velocity scanning methods to define the optimum 1D velocity function as input to the manual velocity picking method (more details mentioned in section 4.2.3.1). Finally, we improve the accuracy of the starting model at shallow depths by inverting surface wave data which carry more details about the very shallow-velocity variations (the method is described at section 4.2.3.2). Once we prepare and enhance the quality of FWI inputs, we perform acoustic FWI over four different frequency bands using both types of objective functions (travel time error and residual which are discussed in more detail in sections 2.5.2 and 2.5.3) and early arrivals then reflection events to reconstruct the fine details without converging to local minima. The FWI strategies of multi-scale and early arrival inversion are summarized in Table 1 at section 4.2.6.

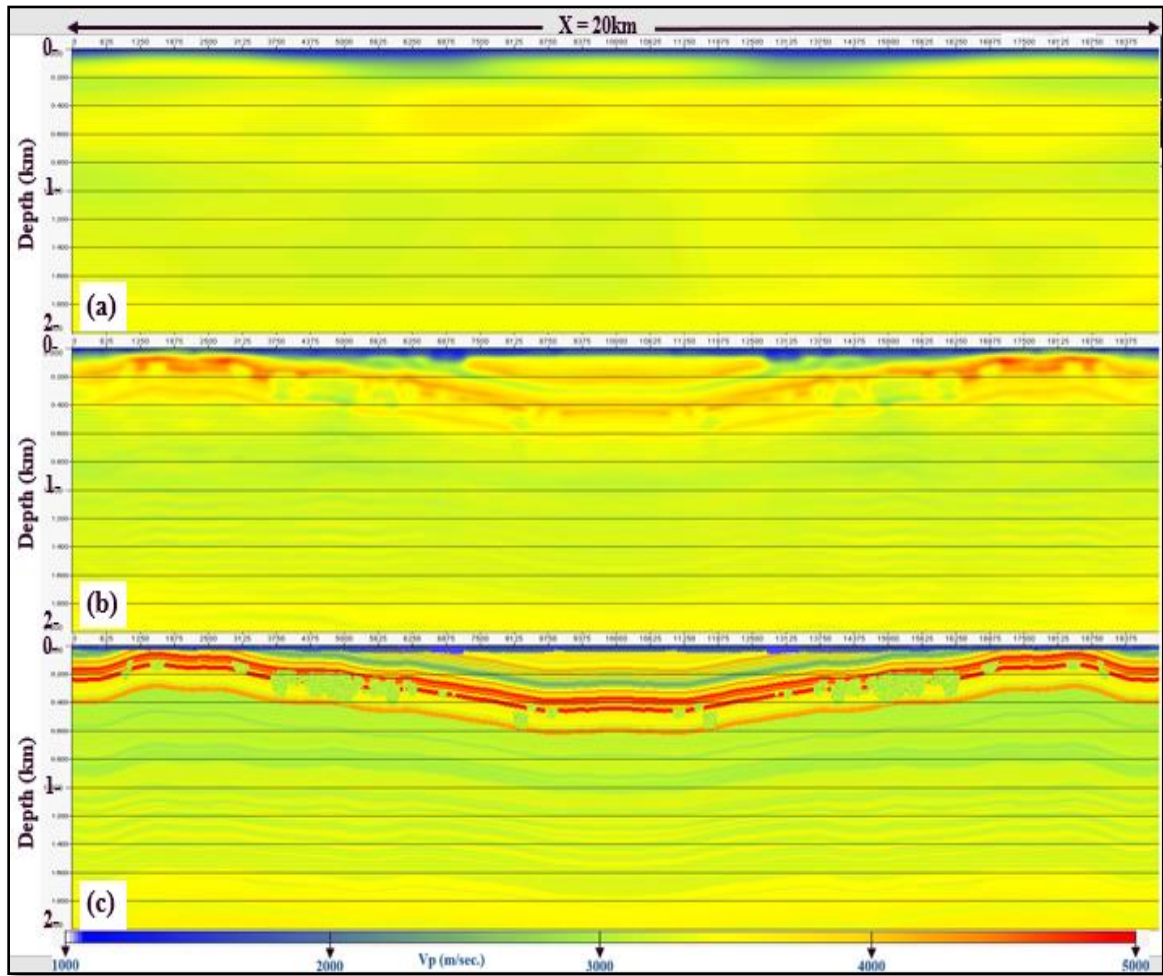


Figure 4-14: P-velocity sections of (a) initial model (b) estimated FWI model (c) true model, shows that acoustic FWI reconstructed successfully the small caves and karst geobodies and low velocity layers.

Figure 4-14 shows acoustic FWI over four frequency bands (4 to 12Hz) on pre-processed viscoelastic data and a more accurate starting model. The inversion successfully reconstructs the small details in the velocity model and estimates more accurately the low-velocity layers and Karst areas at and near the free surface.

Velocity profiles at four locations in the model are shown in Figure 4-15 to illustrate the very good correlation between the estimated model using FWI (red profile) and the true model (black profile).

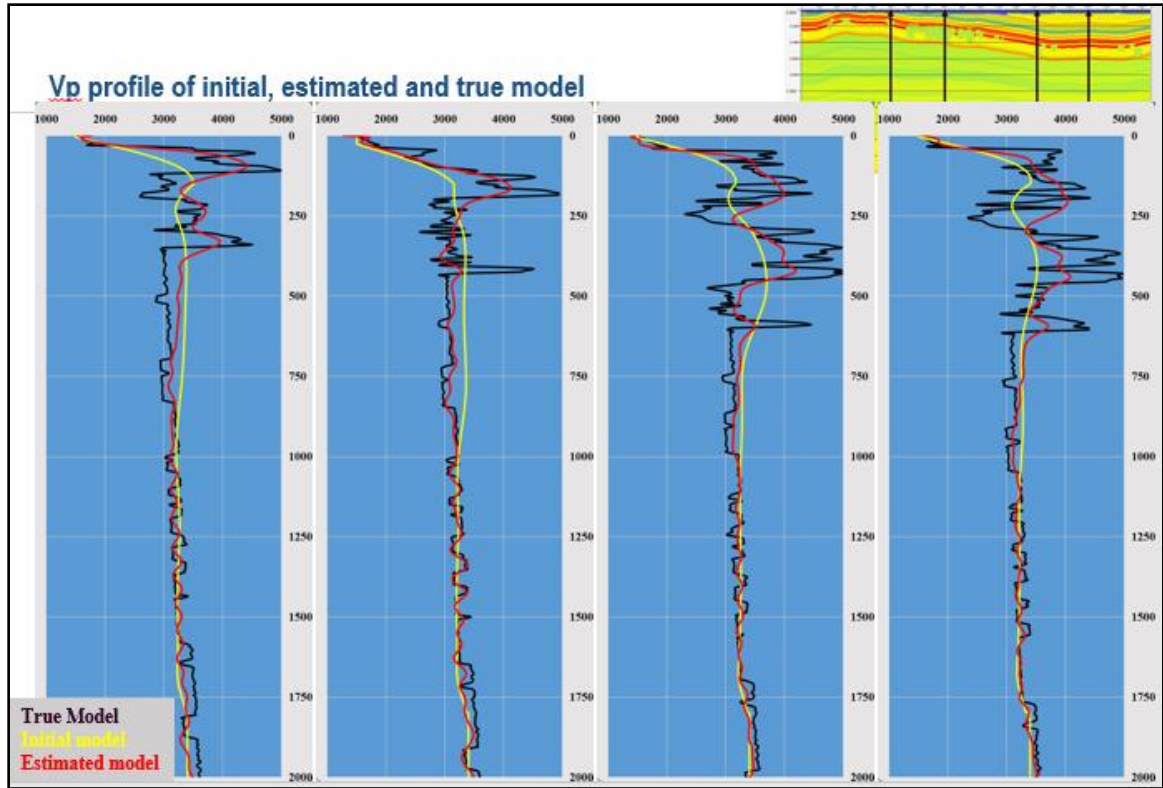


Figure 4-15: velocity profiles extracted at four different locations from the initial model (yellow line), estimated FWI model (red line) and true model (black line), show the similarity between the true and the estimated FWI velocity functions.

RTM images in Figure 4-16 demonstrate the improvement of seismic images due to the accuracy of the reconstructed model by FWI with better continuity of seismic events specially the ones beneath the Karst velocity anomalies.

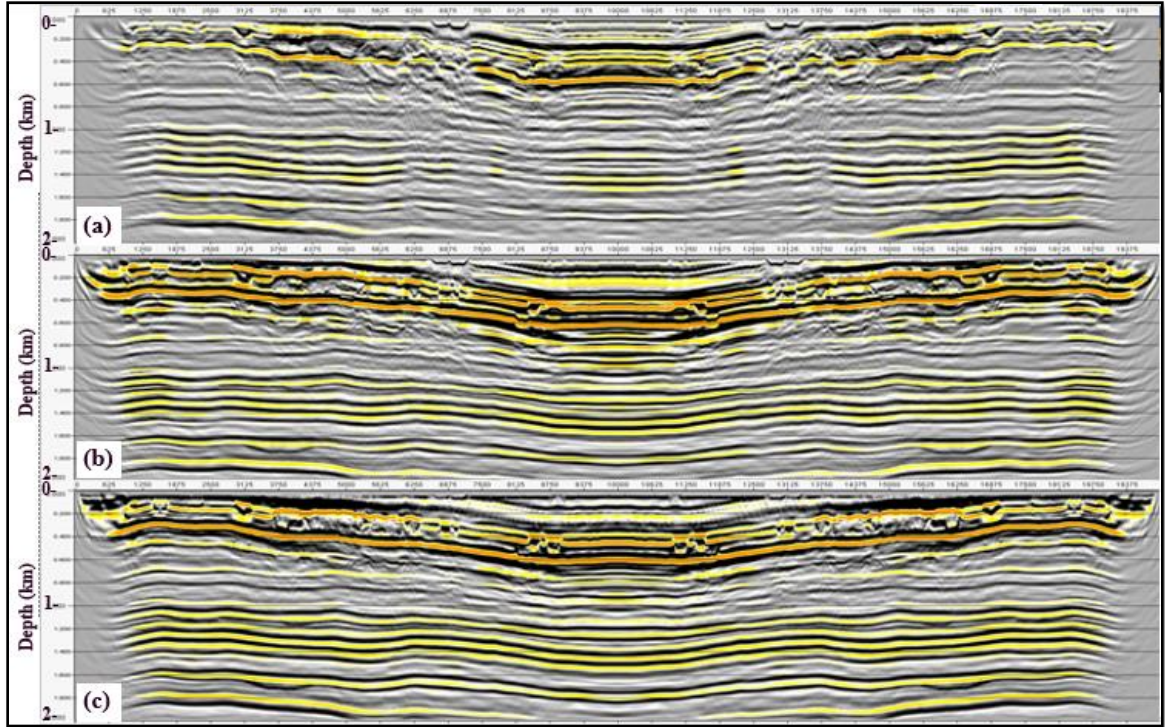


Figure 4-16: RTM Images of different velocity models (a) initial model (b) estimated model (c) true model. RTM images show a clear improvement of subsurface seismic image by using estimated FWI model.

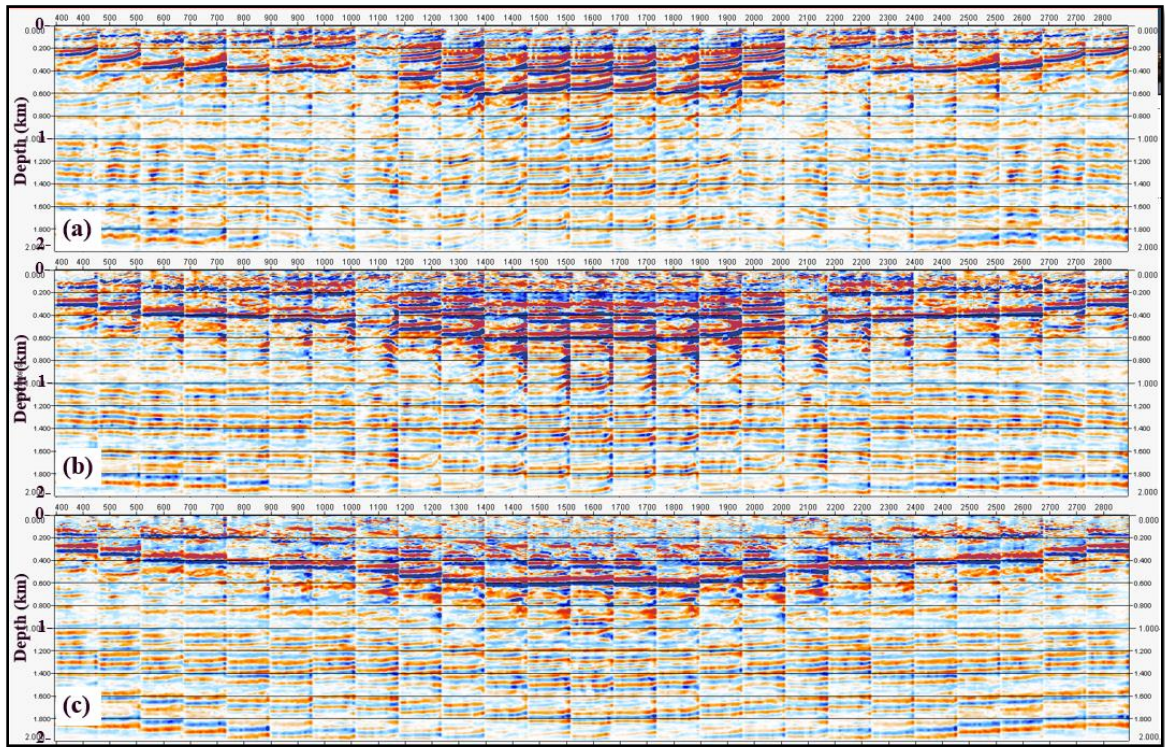


Figure 4-17: RTM gathers of different velocity models (a) initial model (b) estimated FWI model (c) true model, show better flattening of the migrated gathers using the estimated FWI model relative to the migrated gather with the initial model.

RTM angle gathers show better gather flattening and amplitude preservation with angle which will help and post imaging work such as AVO inversion which is vital input for any reservoir characterization study.

4.5 Discussion and conclusion

We showed in this chapter that acoustic FWI can effectively perform and estimate accurate velocities for viscoelastic media providing that careful data conditioning is done on the inputs.

In the data conditioning, I made sure that I take out all the waveforms that cannot be modeled by the acoustic engine. Here, surface waves, scattered shear waves and random noise were removed so that the acoustic FWI does not erroneously take them into the cost function and subsequently use them in the velocity update.

The surface wave inversion was used to estimate the near-surface velocities of the first few hundred meters in the subsurface. This helped the FWI to accurately model the early arrivals from the initial model. The wavelet estimated from the data was thus more reliable. Otherwise the velocity error in the very near-surface could be compensated for by a distortion in the wavelet estimated by FWI.

The two case studies discussed show the importance of the data preparation for acoustic FWI to avoid the problem of cycle skipping and local minimum trapping. The preconditioning of the input gathers and the near-surface velocity estimation reduced this risk.

CHAPTER 5:

Discussion and Conclusions

This thesis report began with an overview in chapter 1 of the challenges of hydrocarbon seismic exploration in complex land environments. It also contains a review of the SEAM program and reflection seismology. At the end of the chapter, I listed the thesis objectives and the expected research contributions.

In chapter 2, I provided more details about the numerical modeling methods, particularly the finite difference scheme which is extensively used in many aspects of forward modeling in seismic exploration. I also presented a summary literature review of the theory of FWI. We highlighted that FWI attempts to reconstruct a subsurface model by minimizing the difference between observed and predicted data in a least square fitting sense and the problem of the inversion getting trapped in a local minimum of the objective function and why this issue is more pronounced with land seismic data. In this chapter, I also introduced the FWI flowchart and methodology, and described in details the main technical components of FWI such as the objective function methods, the cycle skipping problem and computation of the objective function gradient.

We demonstrated in chapter 3 the geological features that are present in the SEAM Phase II Arid model as a realistic representation of the Arabian Peninsula geology. I then evaluated the effect of such complex geological features have on seismic wave propagation through use of a finite difference modeling code and ray tracing experiments. A strong vertical velocity variation causes a discontinuity of the first arrivals which is known as

shingling and produces strong guided waves and internal multiples. Karst at the near-surface and in the subsurface introduces strong velocity contrasts that generate scattered energy which interferes with the reflection of interests and degrades the quality of the seismic data. We addressed further the effect of a complex near-surface geology on different types of seismic wavefields, from acoustic to viscoelastic through forward modeling using the finite difference method which shows strong guided wave with irregular first arrival times, internal multiples and dispersive surface waves due to velocity inversion and complex velocity changes at the near-surface of the Arid SEAM model.

In chapter 4, I discussed the FWI workflow step by step and presented how I processed the FWI input shot gathers to remove all the energy which can't be included in the acoustic modeling. Then I outlined the methodology for determining the starting velocity model using manual velocity picking, in addition to the shallow-velocity update using SWI and its impact on the RTM seismic image. We also discussed our FWI strategies using multiscale and later arrival damping approaches in addition to using different methods for objective function calculations and what conditioning has been done for the gradient. Finally, we presented the FWI results on two different synthetic data one is acoustic and the other is viscoelastic with multiples and noise included.

It is well known that applying FWI to land data is more difficult than marine data especially when the land data has a complex near-surface geology as demonstrated in this thesis. Elastic inversion in such a setting, when only the usual single component data without low frequencies are available, remains a formidable problem for the time being, not only because of the ill-posed nature of determining density, velocity and attenuation of P- and S-waves, and anisotropy all at the same time, but also because of the computational cost of

modeling waves with very small S-velocities. (Mulder & Perkins, 2010). Instead, we utilized seismic processing methods to improve the quality of input data by removing “noise” and increase the accuracy of the starting velocity model to acoustic FWI. This enabled acoustic FWI to effectively work and estimate accurate velocities for viscoelastic media provided that careful data conditioning is done on the inputs.

In the data conditioning, I removed all the waveforms that cannot be modeled by the acoustic engine, such as; surface waves, scattered shear waves and random noise so that the acoustic FWI does not erroneously take them into the cost function and subsequently use them in the velocity update.

The surface wave inversion was used to estimate the near-surface velocities of the top 200m in the subsurface. This helped the FWI to accurately model the early arrivals from the initial model. The wavelet estimated from the data was thus more reliable. Otherwise the velocity error in the very near-surface could be compensated for by a distortion in the wavelet estimated by FWI.

During the application of acoustic FWI, conditioning of the data and updating the velocity using SWI, very careful and detailed analysis and tests were carried out to define the optimum FWI strategy. The strategy was an integration of using different objective function methods, multiscale and later arrival damping FWI approaches. This strategy helped to obtain a successful result of acoustic FWI on viscoelastic data and overcome the local minimum convergence problem which is usually the dominant challenge in such data.

References

- Boonyasiriwat, C., Valasek, P., Routh, P., Cao, W., Schuster, G. T., & Macy, B. (2009). An efficient multiscale method for time-domain waveform tomography. *Geophysics*, 74, WCC59–WCC68.
- Brenders, A. J. and R. G. Pratt (2007a) Efficient waveform tomography for lithospheric imaging: implications for realistic, two-dimensional acquisition geometries and low frequency data. *Geophysical Journal International*, 168, 152–170.
- (2007b) Full waveform tomography for lithospheric imaging: results from a blind test in a realistic crustal model. *Geophysical Journal International*, 168, 133–151.
- (2009) Waveform tomography of 2-D seismic data in the Canadian foothills—data preconditioning by exponential time-damping. In 71st annual international conference and exhibition, EAGE, extended abstracts U041.
- Bunks, C., F. M. Saleck, S. Zaleski, and G. Chavent (1995) Multiscale seismic waveform inversion. *Geophysics*, 60, 1457–1473.
- Claerbout, J. F. (1971) Toward a unified theory of reflector mapping. *Geophysics*, 36, 467–481.
- (1985) *Imaging the earth’s interior*. Blackwell Scientific Publications, Inc.
- (1992) *Earth soundings analysis: Processing versus inversion*. Blackwell Scientific Publications, Inc.
- Chapman, C. (2004) *Fundamentals of seismic wave propagation*. Cambridge University Press.
- Carl Regone, Joseph Stefani, Peter Wang, Constantin Gerea, Gladys Gonzalez, and Crase, E., A. Pica, M. Noble, J. McDonald, and A. Tarantola (1990) Robust elastic nonlinear waveform inversion: Application to real data. *Geophysics*, 55, 527.

- Clayton, R. and B. Engquist (1977) Absorbing boundary conditions for acoustic and elastic wave equations. *Bulletin of the Seismological Society of America*, 67, 1529–1540.
- Denes Vigh, E. William Starr, and Jerry Kapoor (2009) Developing Earth models with full waveform inversion. *The Leading Edge*, 28(4), 432-435.
- Forgues, E., Scala, E., & Pratt, R. G. (1998) High resolution velocity model estimation from refraction and reflection Data. SEG-1998-1211.
- Fichtner, A., Trampert, J., Cupillard, P., Saygin, E., Taymaz, T., Capdeville, Y., et al. (2013) Multiscale full waveform inversion. *Geophysical Journal International*, 194, 534–556.
- Hager, W. W., & Zhang, H. C. (2005) A new conjugate gradient method with guaranteed descent and an efficient line search. *SIAM Journal on Optimization*, 16, 170–192.
- Hoetzi Heinz (1994) Groundwater recharge in an arid karst area (Saudi Arabia). IAHS Publ. no. 232, 1995.
- Kearey, P., Brooks, M., and Hill, I. (2002) *An Introduction to Geophysical Exploration*: Blackwell Science.
- Kun Jiao, Dong Sun, Xin Cheng, and Denes Vigh (2015) Adjustive full waveform inversion. *SEG Technical Program Expanded Abstracts 2015*: pp. 1091-1095.
- Michael Oristaglio (2013) SEAM Update. *The Leading Edge*, 32(6), 606-608.
- (2014) SEAM Update. *The Leading Edge*, 33(7), 710–711.
- (2017) Geologic model building in SEAM Phase II - Land seismic challenges. *The Leading Edge*, 36(9), 738, 740–749.

- Moczo, P., J. O. A. Robertsson and L. Eisner (2007) The finite difference time domain method for modeling of seismic wave propagation: in Advance in wave propagation in heterogeneous Earth. *Advances in geophysics* 48, 421- 516, Elsevier.
- Mulder, W.A. and Plessix, R.-E. (2008) Exploring some issues in acoustic full waveform inversion. *Geophysical Prospecting*, 56: 827–841. doi:10.1111/j.1365-2478.2008.00708.
- Plessix, R.-E. (2006) A review of the adjoint-state method for computing the gradient of a functional with geophysical applications. *Geophysical Journal International*, 167, 495–503.
- Satish Singh, Tim Sears, Mark Roberts, Adam Gosselet, Gillian Royle, and Penny Baton (2008) Full elastic waveform inversion: Future of quantitative seismic imaging. SEG Technical Program Expanded Abstracts 2008: pp. 1905-1909.
- Sheriff, R. E., and Geldart, L. P. (1995) *Exploration Seismology*, Second Edition. Cambridge University Press.
- Strobbia C., Vermeer, P.L., Laake A., Glushchenko, A. and Re S. (2010) Surface waves: processing, inversion and removal. *First Break*, Vol. 28, 85-91.
- Tarantola, A. (1984a) Inversion of seismic reflection data in the acoustic approximation. *Geophysics*, 49, 1259–1266.
- (1984b) Linearized inversion of seismic reflection data. *Geophysical Prospecting*, 32, 998–1015.
- (2005) *Inverse problem theory and methods for model parameter estimation*. SIAM.
- Thorbecke, J. (2013) *Fdelmodc manual*. Technical manual.

Vitae

Name : Ali Ahmed Hussein Mohamed

Nationality : Egyptian

Date of Birth : 7/10/1983

Email : amohamed41@slb.com

Address : Building 61th, 96th street, block 9, Rumaihiya, Kuwait

Academic Background : B.Sc. in Geophysics from Cairo University, Egypt in 2005

Pre-master courses in Seismic Exploration from Cairo University in 2006

List of Publications: Full waveform inversion for complex near-surface imaging using SEG SEAM II model, accepted and presented at Geo2018, Bahrain

Exploring the northern Red Sea - using geological insight and advanced geophysical technologies to unravel the exploration mysteries, accepted for MEOS 2015, Bahrain.

Sub-salt imaging through de-multiple and pre-stack depth migration techniques - A case study from offshore, Mediterranean Offshore Conference, 2009. |